

DOKUZ EYLÜL UNIVERSITY
GRADUATE SCHOOL OF NATURAL AND APPLIED SCIENCES

**LASER FIELD EFFECT ON THE NONLINEAR
OPTICAL PROPERTIES OF QUANTUM DOTS**



by
Selma DURAK

January, 2016

İZMİR

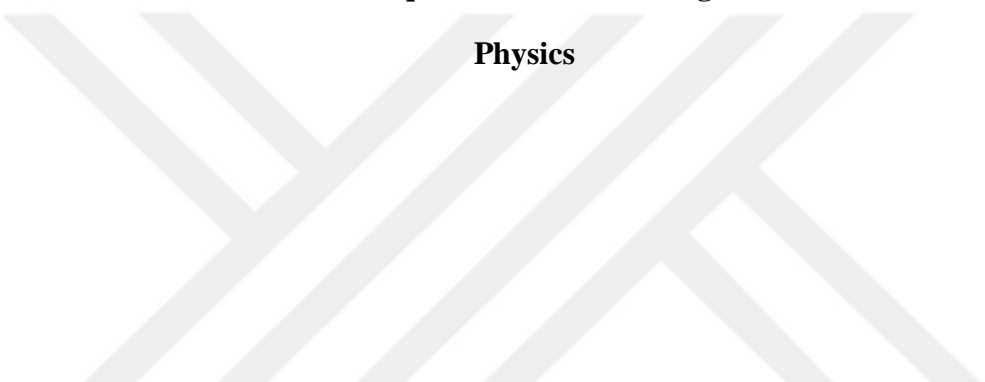
LASER FIELD EFFECT ON THE NONLINEAR OPTICAL PROPERTIES OF QUANTUM DOTS

A Thesis Submitted to the

Graduate School of Natural and Applied Sciences of Dokuz Eylül University

In Partial Fulfillment of the Requirements for the Degree of Master of Science in

Physics



by

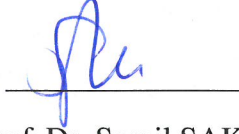
Selma DURAK

January, 2016

İZMİR

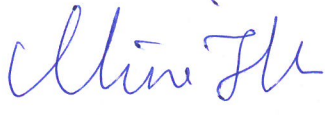
M.Sc THESIS EXAMINATION RESULT FORM

We have read the thesis entitled "**LASER FIELD EFFECT ON THE NONLINEAR OPTICAL PROPERTIES OF QUANTUM DOTS**" completed by **SELMA DURAK** under supervision of **ASSOC. PROF. DR. SERPİL ŞAKİROĞLU** and we certify that in our opinion it is fully adequate, in scope and in quality, as a thesis for the degree of Master of Science.



Assoc. Prof. Dr. Serpil ŞAKİROĞLU

Supervisor



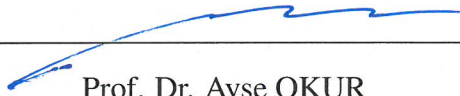
Doç. Dr. Emine Mine ÇAPAR

Jury Member



Prof. Dr. İsmail Sölemcen

Jury Member



Prof. Dr. Ayşe OKUR

Director

Graduate School of Natural and Applied Sciences

ACKNOWLEDGEMENTS

Firstly, I want to state my deepest gratitude to my supervisor Assoc. Prof. Dr. Serpil Şakirođlu for giving me the excellent support to complete this thesis. I'm thankful to her precious guidance, endless patience and valuable help. Her extensive scientific contributions are feasible and invaluable for my academic life.

I'm indebted to Prof. Dr. İsmail Sökmen for extraordinary contributions, innovative recommendations and vital support throughout this work. I'm proud of having the opportunity in his working group. Thanks to him, I learn very crucial knowledges for my academic future in the group.

I must express my special thanks for Prof. Dr. Veysel Kuzucu who is my supervisor in undergraduate. His excellent personality, determined attitude, broad life aspect has profoundly effected my view point. I'm grateful to him for everything which he did.

I request to thank my group friends, who are Necda Çam, Yenal Karaaslan, Dilara Gül, Bircan Gişi, Mehmet Batı and Zeynep Demir, without whose help this project would not have been completed.

I would like to thank my wonderful and lovely family. I can't undergo these days without their paramount support and infinite love. I admit that these couple who are Fatma and Ömer Durak, Merve and Deniz Yiđit, Esra and Necati Kaya are giant importance during my all life. Furthermore, I'm very lucky to have my invaluable brothers Ahmet and Süleyman. Thank you for everything that you have done for me so far.

Finally, I submit The Scientific and Technological Research Council of Turkey (TÜBİTAK)-Münir Bırsel Foundation Graduate Scholarship my thanks for the financially support.

Selma DURAK

LASER FIELD EFFECT ON THE NONLINEAR OPTICAL PROPERTIES OF QUANTUM DOTS

ABSTRACT

In this thesis, we have investigated theoretically the nonlinear optical properties of a two-dimensional Gaussian quantum dot system under a high-frequency intense laser field. The effect of non-resonant monochromatic intense laser field with circular polarization has been taken into account within the framework of non-perturbative approach. The time-dependent Schrödinger equation described the system has been transformed to time-independent form by using the Kramers-Henneberger unitary translational transformation and Fourier-Floquet serial expansion. These approaches lead us to the laser-dressed form of the Gaussian confinement potential.

The compact-density matrix approach and iterative procedure have been used to obtain the nonlinear optical properties of the system. We have studied the laser field effect on the linear and third-order nonlinear optical absorption coefficients and refractive index changes. In order to get numerical solution of the Schrödinger equation, we have used the finite element method with Galerkin approximation.

Numerical results reveal that the structure of the confinement potential is modified remarkably by the laser field. Accordingly, the nonlinear optical properties of the system show a strong dependence on the strength of the high-frequency intense laser field. Moreover, optical absorption coefficients and refractive index changes are affected by the structural parameters.

Keywords: Quantum dot, intense laser field, nonlinear optics, finite element method.

KUANTUM NOKTALARIN LİNEER OLMAYAN OPTİK ÖZELLİKLERİ ÜZERİNE LAZER ALAN ETKİSİ

ÖZ

Bu tezde, yüksek-frekanslı yoğun lazer alanı altındaki iki-boyutlu Gaussian kuantum nokta sisteminin lineer olmayan optik özelliklerini teorik olarak inceledik. Dairesel polarizasyonlu rezonant-olmayan monokromatik yoğun lazer alanının etkisi pertürbatif olmayan yaklaşım çerçevesinde ele alındı. Sistemi tanımlayan zamana-bağlı Schrödinger denklemi, Kramers-Henneberger üniter öteleme dönüşümü ve Fourier-Floquet seri açılımı kullanılarak zamandan-bağımsız forma dönüştürüldü. Bu yaklaşımlar bizi Gaussian hapsedme potansiyelinin lazer-giydirilmiş formuna götürür.

Kompakt-yoğunluk matrisi yaklaşımı ve iteratif şema sistemin lineer olmayan optik özelliklerini elde etmek için kullanıldı. Lineer ve üçüncü-derece lineer olmayan optik soğurma katsayıları ve kırılma indisi değişimleri üzerine lazer alan etkisini çalıştık. Schrödinger denkleminin nümerik çözümlerini elde etmek için Galerkin yaklaşımli sonlu elemanlar yöntemini kullandık.

Nümerik sonuçlar, lazer alanının hapsedme potansiyelinin yapısını önemli ölçüde değiştirdiğini ortaya koymaktadır. Buna bağlı olarak, sistemin lineer olmayan optik özellikleri yüksek-frekanslı yoğun lazer alanın şiddetine güçlü bir bağıllık gösterir. Ayrıca, optik soğurma katsayıları ve kırılma indisi değişimleri yapısal parametreler tarafından etkilenirler.

Anahtar kelimeler : Kuantum nokta, yoğun lazer alanı, lineer olmayan optik, sonlu elemanlar metodu.

CONTENTS

	Page
THESIS EXAMINATION RESULT FORM.....	ii
ACKNOWLEDGEMENTS.....	iii
ABSTRACT.....	iv
ÖZ.....	v
LIST OF FIGURES.....	viii
LIST OF TABLES.....	x
CHAPTER ONE – INTRODUCTION.....	1
CHAPTER TWO – LOW-DIMENSIONAL HETEROSTRUCTURES.....	3
2.1 Introduction to Low-Dimensional Heterostructures.....	3
2.2 Two-Dimensional Structures: Quantum Wells.....	4
2.3 One-Dimensional Structures: Quantum Wires.....	6
2.4 Zero-Dimensional Structures: Quantum Dots.....	6
CHAPTER THREE – THEORETICAL BACKGROUND.....	7
3.1 Theory of Intense Laser Field.....	7
3.2 Finite Element Method.....	9
3.2.1 Solution of Restricted Quantum Systems with FEM.....	10
3.3 Nonlinear Optics.....	14
3.3.1 The Absorption Coefficients and Refractive Index Changes.....	17

CHAPTER FOUR – THE SYSTEM AND METHODOLOGY.....	19
4.1 General Overview of The Problem.....	19
4.2 Theory and Method.....	20
4.3 Dimensionless Form of Hamiltonian.....	22
CHAPTER FIVE – RESULTS AND DISCUSSIONS.....	24
5.1 Effects of Intense Laser Field on The Confining Potential.....	24
5.2 Calculation of Energy Eigenvalues.....	25
5.3 The Effects of Intense Laser Field on The Absorption Coefficients.....	27
5.4 The Effects of Intense Laser Field on The Refractive Index Changes.....	33
CHAPTER SIX – CONCLUSION.....	38
REFERENCES.....	40

LIST OF FIGURES

	Page
Figure 2.1 Illustration of (a) quantum well, (b) quantum wire, and (c) quantum dot....	4
Figure 2.2 Potential energy profile of quantum well	5
Figure 5.1 The confinement potential as a function of r for varying values of (a) depth of the potential and (b) range parameter	24
Figure 5.2 The confinement potential as a function of r for different values of laser- dressing parameter α_0 . We set $V_0 = 200$ meV and $r_0 = 7$ nm	25
Figure 5.3 Bound-state energies as a function of r_0 for the two values of V_0 in case of $\alpha_0 = 0$ nm	26
Figure 5.4 Energies as a function of r_0 for the different values of α_0 with $V_0 = 250$ meV	27
Figure 5.5 The electric dipole moment of the transition between the first state and second state as a function of α_0 for different values of V_0 and r_0	28
Figure 5.6 The energy difference between the first and second states as a function of α_0 for the different values of V_0 and r_0	28
Figure 5.7 Variations of the linear, third-order nonlinear and total AC as a function of the photon energy for the different values of V_0 for $\alpha_0 = 0$ nm, with $r_0 = 10$ nm and $I = 0.3$ MW/cm ²	29
Figure 5.8 Variations of the linear, nonlinear and total AC as a function of the photon energy for the different values of r_0 , for $\alpha_0 = 0$ nm, with $V_0 = 250$ meV and $I = 0.3$ MW/cm ²	30
Figure 5.9 Variations of the linear, nonlinear and total AC as a function of the photon energy for the different values of V_0 , with $r_0 = 7$ nm, $\alpha_0 = 2$ nm and $I = 0.3$ MW/cm ²	30
Figure 5.10 Variations of the linear, nonlinear and total AC as a function of the photon energy for the different values of r_0 . We set $V_0 = 300$ meV, $\alpha_0 = 4$ nm and $I = 0.3$ MW/cm ²	31

Figure 5.11 Variations of the linear, third-order nonlinear and total AC as a function of the photon energy for the different values of α_0 . We use $V_0 = 200$ meV, $r_0 = 15$ nm and $I = 0.3$ MW/cm ²	32
Figure 5.12 Variations of the total AC as a function of the photon energy for the different values of I , with $r_0 = 7$ nm, $V_0 = 300$ meV, $\alpha_0 = 4$ nm	33
Figure 5.13 The linear, nonlinear and total RI changes as a function of the photon energy for different values of V_0 in the absence of laser field. We set $r_0 = 10$ nm and $I = 0.3$ MW/cm ²	34
Figure 5.14 The linear, nonlinear and total RI changes as a function of the photon energy for the different values of r_0 in the absence of laser field. Used parameters are $V_0 = 250$ meV and $I = 0.3$ MW/cm ²	34
Figure 5.15 Laser field-induced changes on the linear, nonlinear and total refractive index as a function of the photon energy for the different values of V_0 with $r_0 = 7$ nm where the laser-dressing parameter is chosen as $\alpha_0 = 2$ nm	35
Figure 5.16 Dependence of the linear, nonlinear and total RI changes on the range parameter r_0 . Potential depth with $V_0 = 300$ meV is chosen and laser-dressing parameter is set to be $\alpha_0 = 4$ nm	36
Figure 5.17 The effect of laser-dressing parameter on the linear, third-order nonlinear and total RI changes as a function of the photon energy. Quantum dot with $V_0 = 200$ meV and $r_0 = 15$ nm is chosen	37
Figure 5.18 The total RI changes as a function of the photon energy for the different values of I , with $r_0 = 7$ nm, $V_0 = 300$ meV, $\alpha_0 = 4$ nm	37

LIST OF TABLES

	Page
Table 3.1 Matrix representation in FEM notation.....	11
Table 5.1 Bound-state energy eigenvalues for Gaussian quantum dot.....	26



CHAPTER ONE

INTRODUCTION

Investigation of electronic and optical properties of low-dimensional semiconductor systems, such as quantum wells, quantum wires, and quantum dots (QDs) has had an enormous interest on account of their importance for practical applications in optoelectronic devices. Especially, owing to their potential application in microelectronics and future laser technology, QDs have reached considerable theoretical and experimental attention (Xie, 2011). The confinement of charge carriers in the low-dimensional semiconductors leads to novel electronic and optical properties which are considerably different from those of the bulk materials. QDs can be selected from low-dimensional semiconductors as a potential candidate for fabricating nanosized devices. The potential applications involve biological probes, lasing media, optical amplifiers, optical sensors and infrared photo-detectors (Saravanamoorthy et al., 2014).

From the point of view of quantum confinement, engineering the electronic structure of materials by means of shape and size control, offers the possibility of tailoring the energy spectrum to fabricate desirable optical transitions (Xie, 2008a). The influence of spatial confinement, which can be formed by introduction of a confinement potential, on the energy spectra of physical systems is one of the most interesting properties to be researched in the study of confined systems (Lu et al., 2011b). When a dot is small (i.e. when its radius is comparable to the characteristic length of the variation of the potential near the edge), a smooth potential such as a Gaussian potential presents a better and more reasonable approximation. The Gaussian potential dot is smooth at the QDs boundaries, which allows us to model a compositional modulation within the QDs (Ehsanfard & Vahdani, 2015).

With the advent of strong coherent tunable laser sources, new possibilities for the study of the interaction of intense laser field (ILF) with nanostructures have emerged. Potential of an electronic system irradiated by an ILF is modified strongly which causes remarkable changes in the electronic and optical properties of the system. The performance of the optoelectronic devices depends on the charge carrier-

electromagnetic radiation interaction. Therefore, it is noteworthy to explore the influence of high-frequency ILF on the optical characteristics in QDs.

Based on the non-perturbative theory that has been developed to describe the atomic behavior in intense high-frequency laser field, several works reported the effects of laser field on the nonlinear optical properties of quantum structures. Generally the presence of an ILF with linear polarization is taken into account through the *laser-dressed potential*. Even though considerable attention has been paid to explore the linearly polarized ILF, less amount of work has been devoted to the effects of circularly polarized ILF-nanostructure interaction.

In this thesis, we survey the effects of circularly polarized high-frequency intense laser field on the optical absorption coefficients (AC) and refractive index changes (RI) of a two-dimensional Gaussian potential quantum dot (2DGPQD). The electronic structure of the system has been calculated by using the finite element method. The nonlinear optical properties have been investigated by using the compact-density matrix approach and iterative procedure. The rest of the thesis is organized as follows: In Chapter 2, low-dimensional heterostructures have been introduced. The theoretical background have been submitted in Chapter 3. In following chapter, the information about the system and the formalism used in this work have been given. In Chapter 5, the numerical results of the system have been demonstrated. Finally, the conclusions has been presented in Chapter 6.

CHAPTER TWO

LOW-DIMENSIONAL HETEROSTRUCTURES

2.1 Introduction to Low-Dimensional Heterostructures

In nanometer scale structures, the motion of an electron can be restricted in one or more directions in space. When only one dimension is confined while the other two remain free the system is called as a quantum well. The structure named quantum wire is formed by a restriction of the electron's motion in two dimensions. Quantum dot is a nanostructure where the charge carriers are restricted in all three dimensions which means zero-degree of freedom. These nanostructures are commonly called low-dimensional quantum structures.

Progress in semiconductor crystal growth technology, such as liquid phase epitaxy, molecular beam epitaxy, metalorganic chemical vapor deposition, has made it possible to control with atomic scale precision the dimensions of semiconductor structures and thus to achieve low-dimensional quantum structures through the formation of heterojunctions or heterostructures. A semiconductor heterojunction is created when two different semiconducting materials are brought into direct contact with each other, while heterostructures can be described as materials that incorporate one or more heterojunctions and can define more complicated device constructions (Razeghi, 2009).

The latest development in the production technology performs the perfect fabrication of dimensional semiconductor quantum nanostructures possible layer by layer in intended geometry. These structures have found a large area of application in many branches of science comprising chemistry, biology, medicine, engineering, and physics. Such materials draw attention of the researchers thanks to their amazing physical properties. Thus, these structures are extensively studied both theoretically and experimentally (Kavruk et al., 2013)

The optical properties of low-dimensional quantum structures, emerging from their peculiar density of states, are often put to use in semiconductor optoelectronic devices, such as semiconductor laser diodes and quantum dot infrared photodetectors. Such low-dimensional structures are generated in practice using a succession of processes including epitaxy, lithography and etc. An illustration of principle of quantum wells, wires and dots is shown in Figure 2.1.

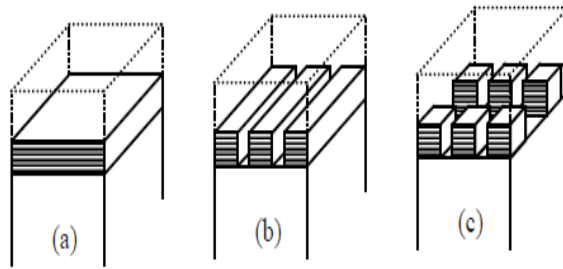


Figure 2.1 Illustration of (a) quantum well, (b) quantum wire, and (c) quantum dot.

Low-dimensional quantum structures have for example been most useful for semiconductor laser diodes, leading to low threshold current (minimum necessary current for lasing), high power and weak temperature dependence devices. These properties, in conjunction with their small size, have made laser diodes attractive for applications including densely packed laser arrays. This implements also to the monolithic integration of lasers with low power electronics such as computer optical interconnects, optoelectronic signal processing and optical computing (Razeghi, 2009).

2.2 Two-Dimensional Structures: Quantum Wells

A quantum well is formed when the motion of electrons is confined in one direction (e.g. x), while it remains free to move in the other two directions (y, z). This situation is most easily obtained by sandwiching a thin and flat film semiconductor crystal between two crystals of another semiconductor material in such a way that a potential step is produced, as shown in Figure 2.2. The electrons are restricted in the region $-L_x/2 < x < L_x/2$. This potential energy profile can be acquired by sandwiching a thin and flat semiconductor of material between two semiconductor crystals of another material.

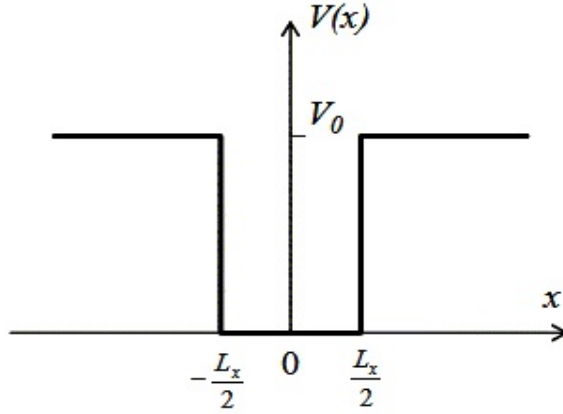


Figure 2.2 Potential energy profile of quantum well.

The potential in the x -direction is similar to the case of a particle in a finite potential well. The height of the potential barrier is now the difference between the conduction band energies in the different semiconductors, which is named the conduction band offset. The contribution to potential in the y - and z -directions is constant and is chosen to be zero, analogous to the case of a free particle. The total potential is given by:

$$V(\vec{r}) = \begin{cases} 0, & \text{for } |x| < L_x/2; \\ V_0 > 0, & \text{for } |x| > L_x/2. \end{cases} \quad (2.1)$$

where \vec{r} includes x -, y - and z -directions. The shape of the potential in Equation 2.1 means that the motion in the x -direction and that in the (y, z) -plane are independent (Razeghi, 2009). The time-independent Schrödinger equation defining the motion of an electron can be written as (Ungan et al., 2010):

$$\left(-\frac{\hbar^2}{2m^*} \nabla^2 + V(\vec{r}) \right) \psi(\vec{r}) = E\psi(\vec{r}) \quad (2.2)$$

where m^* is the electron effective mass. Electronic energies and eigenfunctions can be calculated via the solution of Equation 2.2.

2.3 One-Dimensional Structures: Quantum Wires

A quantum wire is composed when the motion of electrons in the conduction band is confined in two dimensions, while it remains free to move in the remaining direction. This nanostructure can be produced by starting from the result of a quantum well. With a further confinement of quantum well, motion of the charge carriers is allowed only in one dimension. Therefore, one-dimensional quantum structures are obtained (Razeghi, 2009).

2.4 Zero-Dimensional Structures: Quantum Dots

Among the low-dimensional semiconductor structures, a significant attention has been dedicated to the physics of the quantum dots (Khordad, 2012). Quantum dots are nanostructures where the charge carriers are restricted in all three space dimensions and their size, shape and other properties can be controlled in experiments (Xie, 2008b). Modern crystal growth techniques, such as molecular beam epitaxy and metal oxide chemical vapor deposition, have allowed the production of quantum dots with very small dimensions (Khordad, 2012).

Quantum dots have also been named “*artificial atoms*” because their electronic structures and properties resemble those of natural atoms. The reason of this simile is limitation of electrons in quantum dots and atoms due to potential barriers and the Coulomb attraction of the nucleus, respectively (Gomez & Romero, 2009).

Quantum dots confine electrons in all three spatial dimensions and the many-body effects of electron-electron interactions indicate a broad range of electronic structures similar to those of real atoms. Single-electron capacitance spectroscopy offers indirect measurement of the energy levels of a single dot. Since they allow the possibility of applications in future optoelectronic devices and optical memories, it is most interesting to study the electronic structure of QDs (Wen-Fang, 2007; Xie, 2008b).

CHAPTER THREE

THEORETICAL BACKGROUND

3.1 Theory of Intense Laser Field

The study of the interaction of light with atoms, molecules and condensed-matter systems has been the issue of intense research work. The design of new efficient optoelectronic devices depends on understanding of the basic physics of the interaction process. The laser interaction with semiconductor heterostructures has had a private importance in laser works (Brandi et al., 2004).

An atom trapped in a super intense laser field undergoes extreme contortion which results in emergence of exotic appearance. These could not be figured out by using perturbative framework, and requires new (nonperturbative) ideas to be introduced. Considerable progress has thus been devoted to bring out the generation of new atomic structure by means of the high intensities. Along with its fundamental interest, this effort has interesting potential applications (Gavrila, 2002).

To obtain high-intensities one needs to tighten the largest amount of energy possible into the shortest period of time possible (Protopapas et al., 1997). The request for higher and higher laser pulse intensities is driven by some examples, such as nuclear fusion by using lasers. Shorter pulses are required to study fast atomic processes directly in the time domain. As femtosecond (1fs=10⁻¹⁵s) laser technology revolutionized chemistry, the hope is that attosecond (1as=10⁻¹⁸s) laser pulses give a new twist on good old atomic physics (Bauer, 2006).

To examine the motion of particle under radiation field, we need to solve the time-dependent Schrödinger equation that can be expressed as:

$$\left(\frac{(\vec{p} + e\vec{A})^2}{2m^*} + V(\vec{r}) \right) \psi(\vec{r}, t) = i\hbar \frac{\partial \psi(\vec{r}, t)}{\partial t} \quad (3.1)$$

where $\vec{p} = -i\hbar\vec{\nabla}$ is the momentum operator and $\vec{A} = \vec{A}(\vec{r}, t)$ is the vector potential for

the electromagnetic field. For fields that do not vary considerably in the physically important region of space, the dipole approximation can be used which leads to $\vec{A}(\vec{r}, t) \approx \vec{A}(t)$. For any oscillatory $\vec{A}(t)$, we can perform the Kramers-Henneberger unitary translation transformation on Equation 3.1 so as to transfer the time dependence from the kinetic to the potential term in the Hamiltonian of this equation. This unitary transformation is obviously given by the operator (Lima et al., 2009):

$$U = \exp\left[-\frac{i}{\hbar}\left(\frac{e}{m^*} \int \vec{A} \cdot \vec{p} dt + \frac{e^2}{2m^*} \int \vec{A}^2 dt\right)\right] \quad (3.2)$$

This operator can be separated as $U = U_1 U_2$, where $U_1 = \exp\left[-\frac{i}{\hbar}\left(\frac{e}{m^*} \int \vec{A} \cdot \vec{p} dt\right)\right]$ is a translation operator and $U_2 = \exp\left[-\frac{i}{\hbar}\left(\frac{e^2}{2m^*} \int \vec{A}^2 dt\right)\right]$ is an operator that generates a gauge transformation corresponding to the \vec{A}^2 term in the Hamiltonian in Equation 3.1. Within the dipole approximation, however, this term is just a function of t ; thus, it has no physical conclusions and can be transformed away by a shift in the phase of $\psi(\vec{r}, t)$ (Lima et al., 2008). With these operators, the alterations $\varphi(\vec{r}, t) = U^+ \psi(\vec{r}, t)$ and $\tilde{H} = U^+ H U$ lead to:

$$\left(\frac{\vec{p}^2}{2m^*} + V(\vec{r} + \vec{\alpha}(t))\right)\varphi(\vec{r}, t) = i\hbar \frac{\partial \varphi(\vec{r}, t)}{\partial t} \quad (3.3)$$

where $V(\vec{r} + \vec{\alpha}(t))$ is the “*dressed potential*” energy and $\vec{\alpha}(t)$ is commented as a vector corresponding to the classical displacement, along the polarization direction, of the relative particle from its oscillation center. It is expressed as (Sakiroğlu et al., 2012):

$$\vec{\alpha}(t) = \frac{e}{m^*} \int^t \vec{A}(t) dt. \quad (3.4)$$

The dressed potential can be expanded in Fourier-Floquet series. For sufficiently high frequency, the zeroth order Floquet term dominates. For the zeroth Floquet component $\varphi(\vec{r})$, the system degrades to the time-independent Schrödinger equation (Lu et al., 2011b):

$$-\frac{\hbar^2}{2m^*} \nabla^2 \varphi(\vec{r}) + \langle V_d(\vec{r}, \alpha_0) \rangle \varphi(\vec{r}) = E \varphi(\vec{r}) \quad (3.5)$$

where $\langle V_d(\vec{r}, \alpha_0) \rangle$ is the laser-dressed potential given by:

$$\langle V_d(\vec{r}, \alpha_0) \rangle = \frac{1}{T} \int_0^T V(\vec{r} + \vec{a}(t)) dt \quad (3.6)$$

where $T = 2\pi/\omega$ is the period of the laser field (Lima et al., 2009).

3.2 Finite Element Method

In this section, the fundamental methodology of finite element analysis will be introduced. The finite element method can be used so as to analyze various kinds of problems such as structural analysis, heat transfer, fluid flow, mass transport and electromagnetic potential. Especially, any complex shape of problem domain with prescribed conditions can be handled with ease utilizing the finite element method (Young W. Kwon, 1997). Derivation of the finite element equations is shown on a second-order differential equation benefiting the Galerkin approach in a one-dimensional case (Nikishkov, 2010).

The Finite Element Method (FEM) is a procedure for the numerical solution of the equations that govern the problems taken part in nature. Usually the behavior of nature can be described by equations stated in differential or integral form. For this reason, the FEM is understood in mathematical circles as a numerical technique for analyzing partial differential or integral equations. In general, the FEM lets user to obtain the evolution in space and/or time of one or more variables representing the behavior of a physical system (Onate, 2009).

FEM discretization of the problem results in solution of simultaneous algebraic equations. These numerical methods give approximate values of the unknowns at discrete numbers of points in the continuum. Therefore, this process of modeling a body by separating it into in equivalent system of smarter bodies or units (finite elements) interconnected at points common to two or more elements (nodal points or nodes) and/or boundary lines and/or surfaces is called discretization. By using

FEM, we formulate the equations for each finite element and join them to obtain the solution of the entire body instead of resolving the problem for the whole body in one operation (Logan, 2007).

The basic concepts of finite element analysis will be introduced following (Buchanan, 1995):

Interpolation Function:

The basic concept of the finite element method is that a continuous function can be approximated utilizing a discrete model. The discrete model is composed of one or more interpolation polynomials, and the continuous function is separated into finite pieces called elements. Each element is defined using an interpolation function to describe its attitude between its end points. The end points of the finite element are called as nodes.

Shape Functions:

The shape function is generally denoted by the letter N and is usually the coefficient that seems in the interpolation polynomial. A shape function is written for each individual node of a finite element and has the property that its magnitude is 1 at that node and 0 for all other nodes in the element ($\theta_i(x_j) = \delta_{ij}$). The terminology is frequently interchanged between interpolation polynomial and shape function.

3.2.1 Solution of Restricted Quantum Systems with FEM

The Hamiltonian of a charge carrier restricted into a QD, in effective mass approximation, is given by:

$$\mathcal{H} = -\frac{\hbar^2}{2m^*} \nabla^2 + V(\vec{r}) \quad (3.7)$$

where m^* is the effective mass of the charge carrier and $V(\vec{r})$ is the confinement potential (Khordad, 2012). The Bohr radius and effective Hartree energy was used in order to obtain the dimensionless form of Hamiltonian. Consequently, the

dimensionless Hamiltonian is given by:

$$\mathcal{H} = -\frac{1}{2}\nabla_d^2 + V(\vec{r}) \quad (3.8)$$

where the subscript “ d ” represents the dimension of the system. The eigenvalue equation is known as:

$$\mathcal{H}\Psi(\vec{r}) = E\Psi(\vec{r}). \quad (3.9)$$

To find the energy eigenvalues of this equation, we need a trial wave function that defines the physical system. By taking the trial wave function $\psi(\vec{r})$ instead of the wave function $\Psi(\vec{r})$, the Schrödinger equation is translated to:

$$\begin{aligned} \Psi(\vec{r}) \rightarrow \psi(\vec{r}) & \Rightarrow \mathcal{H}\psi(\vec{r}) = E\psi(\vec{r}) \\ (\mathcal{H} - E)\psi(\vec{r}) & \cong 0. \end{aligned} \quad (3.10)$$

The numerical solution of the Equation 3.10 is found by FEM. The first step is that dividing the region of the physical system into subregion. Thus, the wave function is described as a complete set of basis functions ($\theta_i(\vec{r})$) that span the corresponding domain:

$$\psi(\vec{r}) = \sum_{i=1}^{N_{nm}} \psi_i \theta_i(\vec{r}) \quad (3.11)$$

where N_{nm} is the number of total nodes in divided work space. The basis functions (also called shape function or interpolation functions) which span the whole space are often polynomials that are derived using interpolation theory in FEM. The representation of square, column and row matrixes that are used in FEM is shown in Table 3.1.

Table 3.1 Matrix representation in FEM notation.

		FEM
Matrix	$A = \begin{pmatrix} * & * & * \\ * & * & * \\ * & * & * \end{pmatrix}$	$\{\{A\}\}$
Column Matrix	$A = \begin{pmatrix} * \\ * \\ * \end{pmatrix}$	$\{A\}$
Row Matrix	$A = \begin{pmatrix} * & * & * \end{pmatrix}$	$\{A\}^T$

The matrix representation of the Equation 3.11 can be written:

$$\psi(\vec{r}) = \sum_{i=1}^{N_{nm}} \psi_i \theta_i(\vec{r}) = \left\{ \begin{matrix} \psi_1 & \psi_2 & \dots & \psi_{N_{nm}} \end{matrix} \right\} \cdot \left\{ \begin{matrix} \theta_1(\vec{r}) \\ \theta_2(\vec{r}) \\ \vdots \\ \theta_{N_{nm}}(\vec{r}) \end{matrix} \right\} = \{\psi\}^T \{\theta(\vec{r})\} \quad (3.12)$$

$$\psi(\vec{r}) = \{\theta(\vec{r})\}^T \cdot \{\psi\} \quad (3.13)$$

where

$$\{\theta(\vec{r})\}^T = (\theta_1(\vec{r}), \theta_2(\vec{r}), \theta_3(\vec{r}), \dots, \theta_{N_{nm}}(\vec{r})) \quad (3.14)$$

$$\{\psi\}^T = (\psi_1, \psi_2, \psi_3, \dots, \psi_{N_{nm}}) . \quad (3.15)$$

The hermitian conjugate of the wave function is given by:

$$\psi^\dagger(\vec{r}) = \{\psi\}^\dagger \cdot \{\theta(\vec{r})\} . \quad (3.16)$$

In order to derive variational parameters ($\psi_i(\vec{r})$), we can use "Galerkin's Method" (Young W. Kwon, 1997). We obtain G (Galerkian) as:

$$G = \int_{\Omega} \psi^\dagger(\vec{r})(\mathcal{H} - E\mathbf{I})\psi(\vec{r}) d\Omega \quad (3.17)$$

where \mathbf{I} is the unit matrix ($N_{nm} \times N_{nm}$). With using Equation 3.13 and Equation 3.16 in Equation 3.17 the following expression is obtained as:

$$G = \{\psi\}^\dagger \cdot \left[\int_{\Omega} \{\theta\}(\mathcal{H} - E\mathbf{I})\{\theta\}^T d\Omega \right] \cdot \{\psi\} . \quad (3.18)$$

We use the variational method to decide the wave function by minimizing the G expression. A set of wave functions that minimize the Galerkian G and the energy of the system can be found as:

$$\frac{\partial G}{\partial \psi^\dagger} = 0 \quad \Rightarrow \quad \left[\int_{\Omega} \{\theta\}(\mathcal{H} - E\mathbf{I})\{\theta\}^T d\Omega \right] \cdot \{\psi\} = 0 \quad (3.19)$$

When the Hamiltonian expression in Equation 3.8 is inserted in Equation 3.19, we obtain:

$$\left[\int_{\Omega} d\Omega \left(-\frac{1}{2} \{\theta\} \cdot \vec{\nabla}_d^2 \{\theta\}^T + \{\theta\} V(\vec{r}) \{\theta\}^T \right) \right] \cdot \{\psi\} = E \left[\int_{\Omega} d\Omega \{\theta\} \{\theta\}^T \right] \cdot \{\psi\}. \quad (3.20)$$

After the necessary calculations are made, it reads to:

$$\left[\int_{\Omega} d\Omega \left(\frac{1}{2} \vec{\nabla}_d \{\theta\} \cdot \vec{\nabla}_d \{\theta\}^T + \{\theta\} V(\vec{r}) \{\theta\}^T \right) \right] \cdot \{\psi\} = E \left[\int_{\Omega} d\Omega \{\theta\} \{\theta\}^T \right] \cdot \{\psi\}. \quad (3.21)$$

The Equation 3.21 can be expressed in more compact notation as follows:

$$\{\{K\}\} \cdot \{\psi\} = E \{\{M\}\} \cdot \{\psi\} \quad (3.22)$$

where $\{\{K\}\}$ is “*Stiffness Matrix*” and $\{\{M\}\}$ is “*Mass Matrix*”. A representation of generalized eigenvalue equation of the system is shown in Equation 3.22. The stiffness matrix $\{\{K\}\}$ is a coefficient matrix whose elements do not contain the energy term, while the mass matrix $\{\{M\}\}$ is a coefficient matrix in the right hand side of the generalized eigenvalue equation. The matrices are given by:

$$\{\{K\}\} = \int_{\Omega} d\Omega \left(\frac{1}{2} \vec{\nabla}_d \{\theta\} \cdot \vec{\nabla}_d \{\theta\}^T + \{\theta\} V(\vec{r}) \{\theta\}^T \right) \quad (3.23)$$

$$\{\{M\}\} = \int_{\Omega} d\Omega \{\theta\} \{\theta\}^T. \quad (3.24)$$

With a division of the whole workspace into a global elements, the integral over the Ω is written as a summation of the integrals over the subinterval space elements. That is:

$$\int_{\Omega} d\Omega = \sum_{e=1}^{N_e} \int_{\Omega_e} d\Omega_e \quad (3.25)$$

where N_e is the number of the global elements. Therefore, we define the stiffness and mass matrices as:

$$\{\{K\}\} = \sum_{e=1}^{N_e} \{\{k_e\}\} \quad (3.26)$$

$$\{\{k_e\}\} = \int_{\Omega_e} d\Omega_e \left(\frac{1}{2} \vec{\nabla}_d \{N\} \cdot \vec{\nabla}_d \{N\}^T + \{N\} V(\vec{r}) \{N\}^T \right). \quad (3.27)$$

In Equation 3.27, $\{\{k_e\}\}$ matrix contains both the kinetic and potential energy term.

$$\{\{k_e\}\} = \{\{k_{e,kin}\}\} + \{\{k_{e,pot}\}\}$$

$$\{\{k_{e,kin}\}\} = \int_{\Omega_e} d\Omega_e \left(\frac{1}{2} \vec{\nabla}_d \{N\} \vec{\nabla}_d \{N\}^T \right) \quad (3.28)$$

$$\{\{k_{e,pot}\}\} = \int_{\Omega_e} d\Omega_e (\{N\} V \{N\}^T) \quad (3.29)$$

$$\{\{M\}\} = \sum_{e=1}^{N_e} \{\{m_e\}\} \quad (3.30)$$

$$\{\{m_e\}\} = \int_{\Omega_e} d\Omega_e \{N\} \{N\}^T. \quad (3.31)$$

where $\{N\}$ represents the global element basis function (Sarikurt, 2013).

3.3 Nonlinear Optics

Light seems to flow and propagate through empty space, as well as through solid matters and maintains us with visual information about our planet. The similar effects of reflection, refraction, diffraction, absorption and scattering identify a wide variety of visual experiences common to us, from the focusing of light by a simple lens to the colors seen in a rainbow. Significantly, these can be clarified by assigning a small set of optical parameters to materials. Under the daily routine of every day life, these parameters are constant, independent of the intensity of light that allows observation of the optical phenomena. This is the fundamental of linear optics.

The optic researches at high intensities have been expanded with the invention of laser sources. The high intensities of the laser field lead to new phenomena which is not seen in ordinary light such as the generation of new colors from monochromatic light in a transparent crystal or the self-focusing of an optical beam in a homogeneous

liquid. At sufficiently strong intensities, the general optical parameters of matters can not be considered as a constant anymore, much rather they become functions of the light intensity. The optics in this form is called nonlinear optics (Sutherland, 2003).

Nonlinear optics is the study of phenomena that emerges as a consequence of the modification of the optical properties in a system by the existence of the light. Generally, only laser light is adequately intense to modify the optical properties of a material system (Boyd, 2008). Nonlinear optics is the discipline in physics in which the electric polarization density of the medium is searched as a nonlinear function of the electromagnetic field of the light. Being a wide field of investigation in electromagnetic wave propagation, nonlinear interaction between light and matter leads to a wide spectrum of phenomena, such as optical frequency conversion, optical solution, phase conjugation, and Raman scattering. Moreover, many of analytical tools implemented in nonlinear optics are of general character, such as the perturbative techniques and symmetry considerations, and can even well be implemented in other disciplines in nonlinear dynamics (Jonsson, 2003). Practical nonlinear optical tools in semiconductors are on the verge of becoming a reality, as switches, modulators, converters and sensors (Garmire & Kost, 1999).

The theory of nonlinear optics constructs on the well-understood theory of linear optics. It is related to interaction of light and matter. Ordinary matter consists of a combination of positively charged cores envionred with negatively charged electrons. Light interacts principally with the matter via the valence electrons in the outhter shells of electron orbitals which causes to an electronic polarization. This is the main parameter for nonlinear optics. Expanding the description of this parameter to the nonlinear regime consents the definition of a rich variety of optical phenomena at high intensity (Sutherland, 2003).

We assume that the interaction of polarized monochromatic electromagnetic field with the 2DGPQD. The electric field vector of the optical wave is (Mills, 1998):

$$\vec{E}(t) = \vec{E}_0 \cos(\omega t) = \vec{E} e^{-i\omega t} + \vec{E}^* e^{+i\omega t}. \quad (3.32)$$

The time evolution of the matrix elements of one-electron density operator is given by (Ehsanfard & Vahdani, 2015):

$$\frac{\partial \hat{\rho}}{\partial t} = \frac{1}{i\hbar} [\hat{H}_0 - e\vec{r} \cdot \vec{E}(t), \hat{\rho}] - \Gamma (\hat{\rho} - \hat{\rho}^{(0)}) \quad (3.33)$$

where \hat{H}_0 is the Hamiltonian of the system in the absence of electromagnetic field, e is the electric charge, $\hat{\rho}$ is the density matrix of single electron state, $\hat{\rho}^{(0)}$ is the unperturbed density operator, Γ is the phenomenological relaxation rate, caused by the electron-phonon, the electron-electron and the other collision processes. Equation 3.33 can be solved using the iterative method by expanding $\hat{\rho}$ (Gül, 2014):

$$\hat{\rho}(t) = \sum_{n=0}^{\infty} \hat{\rho}^{(n)} \quad (3.34)$$

with

$$\frac{\partial \hat{\rho}_{ij}^{(n+1)}}{\partial t} = \frac{1}{i\hbar} \{ [\hat{H}_0, \hat{\rho}^{(n+1)}]_{ij} - i\hbar \Gamma_{ij} \hat{\rho}_{ij}^{(n+1)} \} - \frac{1}{i\hbar} [\hat{M}, \hat{\rho}^{(n)}]_{ij} \cdot \vec{E}(t) \quad (3.35)$$

can be found perturbation solution of Equation 3.33 and where $\hat{M} = e\vec{r}$ is the electric dipole moment operator (Liu et al., 2012).

The electronic polarization given by (Tiutiunnyk et al., 2014):

$$P(t) = \frac{1}{S} Tr(\hat{\rho}\hat{M}) = \chi(\omega)E(t) \quad (3.36)$$

where $\chi(\omega)$ is the dielectric susceptibility, S is the total area of the system and the symbol Tr (trace) denotes summation over the diagonal elements of the matrix $\hat{\rho}\hat{M}$. Hence, the polarization can be written as:

$$P(t) = \epsilon_0 \chi_{(\omega)}^{(1)} \tilde{E} e^{i\omega t} + \epsilon_0 \chi_{(2\omega)}^{(2)} \tilde{E}^2 e^{2i\omega t} + \epsilon_0 \chi_{(3\omega)}^{(3)} \tilde{E}^3 e^{3i\omega t} + c.c \quad (3.37)$$

where ϵ_0 is the vacuum permittivity and $\chi_{(\omega)}^{(1)}$, $\chi_{(2\omega)}^{(2)}$ and $\chi_{(3\omega)}^{(3)}$ are the linear, the second-order and the third-order nonlinear optical susceptibilities, respectively. We don't consider the second-order nonlinear term because in geometries with reflective

symmetry center the second order polarization is equal to zero and thus, in our geometry the second order nonlinear optical properties are not anticipated (Safarpour et al., 2014).

3.3.1 *The Absorption Coefficients and Refractive Index Changes*

Absorption is the basic physical process in the working of solar cells, infrared photodetectors and many alike optical devices. Therefore, understanding of the optical absorption in such structures is crucial in the production of new generation high technology devices. For instance, the energy levels and depending on these, the resonant absorption wavelength can be tuned via size of the QD or combinations of the QD materials. Nonlinear optical properties are as significant as the linear ones in the device fabrication (Kavruk et al., 2013).

To calculate the absorption coefficient for a dressed quantum dot corresponding to an optical transition between two subbands we have utilized the compact density matrix method and the usual iterative procedure (Niculescu & Burileanu, 2010).

The optical susceptibility $\chi(\omega)$ is related to the absorption coefficient $\alpha(\omega)$ by (Xie, 2010a):

$$\alpha(\omega) = \omega \sqrt{\frac{\mu}{\epsilon_R}} \text{Im}[\epsilon_0 \chi(\omega)] \quad (3.38)$$

where μ is the magnetic permeability of vacuum, and $\epsilon_R = n_r^2 \epsilon_0$ is the real part of the permittivity. Therefore, the linear and nonlinear optical absorption coefficients (Ozturk & Sokmen, 2014; Duque et al., 2013; Ahn & Chuang, 1987):

$$\alpha^{(1)}(\omega) = \omega \sqrt{\frac{\mu}{\epsilon_R}} \frac{\sigma_v \hbar \Gamma_{if} |M_{fi}|^2}{(E_{fi} - \hbar \omega)^2 + (\hbar \Gamma_{if})^2} \quad (3.39)$$

$$\alpha^{(3)}(\omega, I) = -\omega \sqrt{\frac{\mu}{\epsilon_R}} \frac{I}{2 \epsilon_0 n_r c} \frac{\sigma_v \hbar \Gamma_{if} |M_{fi}|^2}{[(E_{fi} - \hbar\omega)^2 + (\hbar\Gamma_{if})^2]^2} \quad (3.40)$$

$$x \left\{ 4 |M_{fi}|^2 - \frac{|M_{ff} - M_{ii}|^2 [3 E_{fi}^2 - 4 E_{fi} \hbar \omega + \hbar^2 (\omega^2 - \Gamma_{if}^2)]}{E_{fi}^2 + (\hbar\Gamma_{if})^2} \right\}$$

where $E_{fi} = E_f - E_i$ is the transition energy difference between the initial i and final f energy states, $\hat{M}_{fi} = e\langle f|\vec{r}|i\rangle$ is the electric dipole moment of the transition from i state to f state, ϵ_0 is the free-space dielectric permittivity, c is the speed of light in vacuum, n_r is the refractive index of the material, σ_v is the carrier density, and $I = 2\epsilon_0 n_r c |E|^2$ is the optical intensity of the incident electromagnetic wave. The total optical absorption coefficient is given by:

$$\alpha^{(T)}(\omega, I) = \alpha^{(1)}(\omega) + \alpha^{(3)}(\omega, I). \quad (3.41)$$

The optical susceptibility $\chi(\omega)$ is related to the change in the refractive index as (Lu et al., 2011a):

$$\frac{\Delta n(\omega)}{n_r} = \text{Re} \left(\frac{\chi(\omega)}{2 n_r^2} \right). \quad (3.42)$$

Thus, the linear and nonlinear changes in the refractive index are written as (Ozturk & Sokmen, 2014; Duque et al., 2013; Ahn & Chuang, 1987):

$$\frac{\Delta n^{(1)}(\omega)}{n_r} = \frac{\sigma_v |M_{fi}|^2}{2 \epsilon_R} \frac{E_{fi} - \hbar \omega}{(E_{fi} - \hbar \omega)^2 + (\hbar \Gamma_{if})^2} \quad (3.43)$$

$$\frac{\Delta n^{(3)}(\omega, I)}{n_r} = -\frac{\sigma_v \mu c I |M_{fi}|^2}{4 \epsilon_R} \frac{E_{fi} - \hbar \omega}{[(E_{fi} - \hbar \omega)^2 + (\hbar \Gamma_{if})^2]^2} \quad (3.44)$$

$$x \left\{ 4 |M_{fi}|^2 - \frac{(M_{ff} - M_{ii})^2}{E_{fi}^2 + (\hbar \Gamma_{if})^2} \left[E_{fi}(E_{fi} - \hbar \omega) - (\hbar \Gamma_{if})^2 - \frac{(\hbar \Gamma_{if})^2 (2 E_{fi} - \hbar \omega)}{E_{fi} - \hbar \omega} \right] \right\}$$

Accordingly, the total refractive index is that:

$$\frac{\Delta n^{(T)}(\omega, I)}{n_r} = \frac{\Delta n^{(1)}(\omega)}{n_r} + \frac{\Delta n^{(3)}(\omega, I)}{n_r}. \quad (3.45)$$

CHAPTER FOUR

THE SYSTEM AND METHODOLOGY

4.1 General Overview of The Problem

Laser field effect on the nonlinear optical properties of quantum dots is an attractive research subject. Several works have been devoted to understand the optical characteristics of quantum dots. Zhang et al. have investigated the influence of intense laser field on the energy states and optical properties induced by sublevel transitions of the cylinder quantum dot system considering the piezoelectric effect (Zhang et al., 2011). Xie et al. have performed an investigation of the influence of a laser field on the electron-hole excitations in disc-like quantum dot with parabolic potential. They reported the absorption spectra and the refractive indexes by using the matrix diagonalization and the compact density-matrix methods (Xie, 2011). Lu et al. have theoretically searched the effects of intense laser fields on the nonlinear properties of donor impurities in a quantum dot with Woods-Saxon potential within the matrix diagonalization method with the use of the effective mass approximation. In their work, the intense laser effects are taken into account through the Floquet method, by modifying the confining potential associated to the heterostructure (Lu et al., 2011a). Safarpour et al. have investigated the linear, third-order nonlinear and total optical absorption coefficients and refractive index changes of a *GaAs* spherical quantum dot placed at the center of a *Ga_{1-x}Al_xAs* cylindrical nano-wire. In this work, the finite difference approximation is considered in calculation of the electronic structure as well as compact density-matrix approach is applied to investigate the optical properties (Safarpour et al., 2014). Lu et al. have researched optical properties of donor impurities in quantum dots under the influence of a linearly polarized laser field with Gaussian potential by using the matrix diagonalization method within the effective mass approximation (Lu et al., 2011b).

In spite of different works about optical properties in quantum dots under laser field, linearly polarized ILF is used in most of them. The nonlinear optical properties of

two-dimensional Gaussian quantum dot system exposed to circularly polarized high-frequency intense laser field have not been investigated so far. Therefore in this thesis, we focus on the survey of optical properties of this structure.

4.2 Theory and Method

The approach used in the present calculation is based upon a non-perturbative theory that has been developed to define the atomic behavior in intense high-frequency laser fields. The radiation field can be offered by a monochromatic plane wave. We shall be interested here in the case of circularly polarized laser field. The vector potential can be taken as:

$$\vec{A}(t) = A_0(\hat{x} \cos \Omega t - \hat{y} \sin \Omega t) \quad (4.1)$$

and correspondingly the vector $\vec{\alpha}(t)$ calculated by using Equation 3.4 is:

$$\vec{\alpha}(t) = \alpha_0(\hat{x} \sin \Omega t + \hat{y} \cos \Omega t) . \quad (4.2)$$

Here \hat{x} and \hat{y} are the unit vectors along the x - and y -axes, respectively, Ω is the angular frequency of the laser field (Miyagi & Someda, 2009, Pont & Gavrilu, 1990). $\alpha_0 = \frac{eA_0}{m^*c\Omega}$, called as laser-dressing parameter, represents for the quiver motion of a classical electron in the laser field and A_0 is the amplitude of the vector potential (Ungan et al., 2010).

The knowledge of confinement potential profile in QDs has an crucial role in physics of semiconductor structures. Quantum confinement potentials which restrict the charge carriers in QDs have various shapes depending on origin and structure of the QD (Khordad, 2012). We choose the potential form of a quantum dot (QD) as a Gaussian potential, which is given by (Xie, 2010b):

$$V_G(r) = -V_0 \exp\left(-\frac{r}{r_0}\right)^2 \quad (4.3)$$

where $V_0 > 0$ is the depth of the potential dot, r_0 is the range of the confinement

potential describing the radius of the QD, and r contains x and y coordinates. In order to obtain the laser-dressed Gaussian potential, we apply initially the time-dependent translation $\vec{r} \rightarrow \vec{r} + \vec{\alpha}(t)$ to the potential. By simple algebra the potential is translated to:

$$V_G(\vec{r} + \vec{\alpha}(t)) = -V_0 \exp\left[-\frac{r^2 + 2r\alpha_0 \cos(u - \phi) + \alpha_0^2}{r_0^2}\right] \quad (4.4)$$

where $u = \Omega t$ is a variable chosen for simplicity and ϕ is angle between \vec{r} and $\vec{\alpha}(t)$. If Equation 4.4 is inserted in Equation 3.6, we obtain the laser-dressed Gaussian potential as:

$$\langle V_{Gdressed}(\vec{r}, \alpha_0) \rangle = -\frac{V_0}{2\pi} \int_0^{2\pi} \exp\left[-\frac{(r^2 + \alpha_0^2)}{r_0^2}\right] \exp\left[-\frac{2r\alpha_0 \cos(u - \phi)}{r_0^2}\right] du \quad (4.5)$$

Terms independent of variable u are taken in front of the integral which leads to:

$$\langle V_{Gdressed}(\vec{r}, \alpha_0) \rangle = -\frac{V_0}{2\pi} \exp\left[-\frac{(r^2 + \alpha_0^2)}{r_0^2}\right] \int_0^{2\pi} \exp\left[-\frac{2r\alpha_0 \cos(u - \phi)}{r_0^2}\right] du \quad (4.6)$$

Using the Jacobi-Anger expansion (Colton & Kress, 1998):

$$\exp(iz \cos \theta) = \sum_{n=-\infty}^{\infty} i^n J_n(z) \exp(in\theta), \quad (4.7)$$

and taking as $a = \frac{2r\alpha_0}{r_0^2}$, we get:

$$\langle V_{Gdressed}(\vec{r}, \alpha_0) \rangle = -\frac{V_0}{2\pi} \exp\left[-\frac{(r^2 + \alpha_0^2)}{r_0^2}\right] \sum_{n=-\infty}^{\infty} i^n J_n(ia) 2\pi e^{-in\phi} \delta_{n,0} \quad (4.8)$$

$\delta_{n,0}$ denotes kronecker delta operator. Hence, the summation in Equation 4.8 drops which yields to the new form of the dressed potential:

$$\langle V_{Gdressed}(\vec{r}, \alpha_0) \rangle = -\frac{V_0}{2\pi} \exp\left[-\frac{(r^2 + \alpha_0^2)}{r_0^2}\right] 2\pi J_0(ia) \quad (4.9)$$

Modified Bessel function (Hanna & Rowland, 2008) is defined as:

$$I_\alpha(x) = i^{-\alpha} J_\alpha(ix). \quad (4.10)$$

Using the relation between Bessel functions, the final form of the laser-dressed Gaussian potential is obtained to be:

$$\langle V_{Gdressed}(\vec{r}, \alpha_0) \rangle = -V_0 \exp\left[-\frac{(r^2 + \alpha_0^2)}{r_0^2}\right] I_0\left(\frac{2\alpha_0 r}{r_0}\right). \quad (4.11)$$

Here, I_0 is the modified Bessel function for $\alpha = 0$.

4.3 Dimensionless Form of Hamiltonian

We need dimensionless form of Equation 3.5 for numerical solution of the system. We use effective Hartree energy $E_h^* = \frac{\hbar^2}{m^*(a_0^*)^2}$ and effective Bohr radius $a_0^* = \frac{4\pi\epsilon_0\epsilon_r\hbar^2}{m^*e^2}$ as the energy and length scales, respectively. Therefore, the variables and parameters in the Hamiltonian can be written in terms of these units: $r \rightarrow a_0^*\tilde{r}$, $V_0 \rightarrow E_h^*\tilde{V}_0$ and $\alpha_0 \rightarrow a_0^*\tilde{\alpha}_0$. The dimensionless form of laser-dressed Gaussian potential becomes:

$$\langle \tilde{V}_{Gdressed}(\tilde{r}, \tilde{\alpha}_0) \rangle = -\tilde{V}_0 \exp\left[-\frac{(\tilde{r}^2 + \tilde{\alpha}_0^2)}{\tilde{r}_0^2}\right] I_0\left(\frac{2\tilde{\alpha}_0\tilde{r}}{\tilde{r}_0}\right). \quad (4.12)$$

For convenience, we use the abbreviation $\tilde{V}_{GD} = \langle \tilde{V}_{Gdressed}(\tilde{r}, \tilde{\alpha}_0) \rangle$. As taking $\tilde{E} = E/E_h^*$, dimensionless eigenvalue equation can express as:

$$\tilde{H}\psi(\tilde{r}, \theta) = \tilde{E}\psi(\tilde{r}, \theta) \quad (4.13)$$

$$-\frac{1}{2}\tilde{\nabla}^2\psi(\tilde{r}, \theta) + \tilde{V}_{GD}\psi(\tilde{r}, \theta) = \tilde{E}\psi(\tilde{r}, \theta). \quad (4.14)$$

The wavefunction $\psi(\tilde{r}, \theta)$ can be decomposed as $\psi(\tilde{r}, \theta) = R(\tilde{r})\Theta(\theta)$. By solving the equation for two-dimension, the new expression transform into:

$$-\frac{1}{2}\left[\frac{1}{\tilde{r}}\frac{\partial}{\partial\tilde{r}}\left(\tilde{r}\frac{\partial}{\partial\tilde{r}}\right) + \frac{1}{\tilde{r}^2}\frac{\partial^2}{\partial\theta^2}\right]R(\tilde{r})\Theta(\theta) + \tilde{V}_{GD}R(\tilde{r})\Theta(\theta) = \tilde{E}R(\tilde{r})\Theta(\theta). \quad (4.15)$$

When the necessary operations are made, Equation 4.15 converts to:

$$-\frac{1}{2}\left[\frac{1}{\tilde{r}R(\tilde{r})}\frac{d}{d\tilde{r}}\left(\tilde{r}\frac{dR(\tilde{r})}{d\tilde{r}}\right) + \frac{1}{\tilde{r}^2\Theta(\theta)}\frac{d^2\Theta(\theta)}{d\theta^2}\right] + \tilde{V}_{GD} = \tilde{E} \quad (4.16)$$

where $\Theta(\theta) = \frac{1}{\sqrt{2\pi}}e^{im\theta}$ is the radial part of the two-dimensional wavefunction and m is orbital angular momentum magnetic quantum number. By making some calculations, consequently, the eigenvalue equation of the system is:

$$-\frac{1}{2} \left[\frac{1}{\tilde{r}} \frac{d}{d\tilde{r}} \tilde{r} \frac{d}{d\tilde{r}} - \frac{m^2}{\tilde{r}^2} \right] R(\tilde{r}) + \tilde{V}_{GD} R(\tilde{r}) = \tilde{E} R(\tilde{r}). \quad (4.17)$$

We have acquired numerical results for Equation 4.17 by utilizing FEM. In the calculations, we work with 1000 nodes as a number of total nodes, and 10 nodes as a number of global nodes.



CHAPTER FIVE

RESULTS AND DISCUSSIONS

5.1 Effects of Intense Laser Field on The Confining Potential

In this section of the work, we discuss changes of the potential profile with respect to the structure parameters. The potential profiles are demonstrated as a function of radial coordinate r for different values of potential depth V_0 , range parameter r_0 and laser-dressing parameter α_0 .

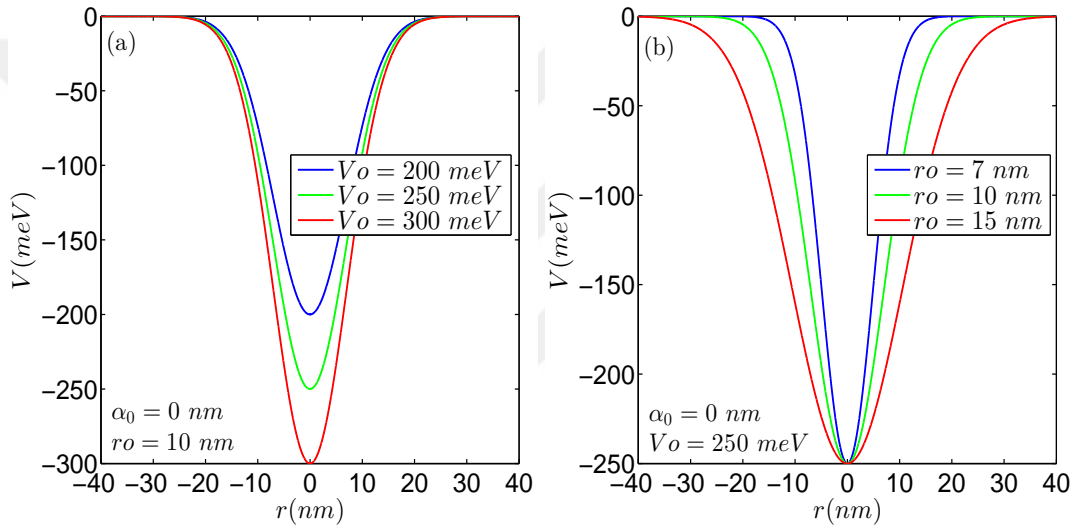


Figure 5.1 The confinement potential as a function of r for varying values of (a) depth of the potential and (b) range parameter.

Figure 5.1 displays the confinement potential for different values of (a) V_0 for $r_0 = 10$ nm and (b) r_0 for a constant $V_0 = 250$ meV considering absence of intense laser field ($\alpha_0 = 0$ nm). It shows clearly that for increasing V_0 values the potential becomes deeper while for increasing radius r_0 the effective width of the confinement potential expands.

In Figure 5.2, we have plotted variation of the Gaussian confining potential for different values of laser-dressing parameter α_0 for $V_0 = 200$ meV and $r_0 = 7$ nm. The figure shows clearly that as the value of α_0 increases the width of the confinement potential expands and furthermore, the depth of potential decreases.

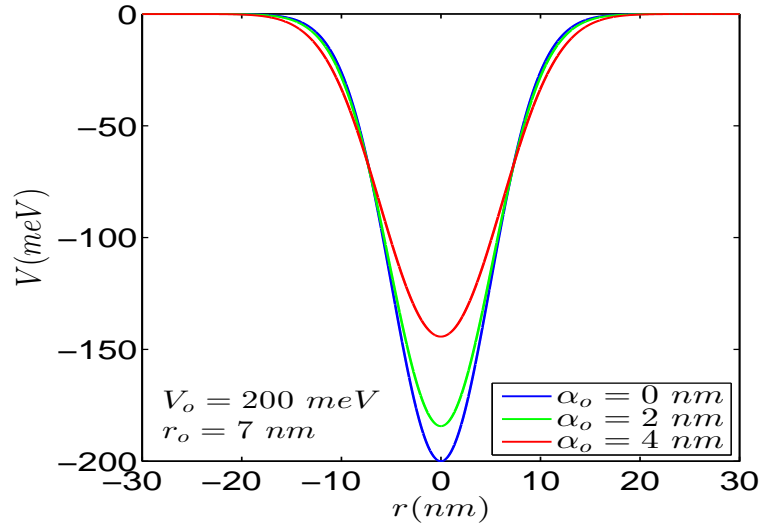


Figure 5.2 The confinement potential as a function of r for different values of laser-dressing parameter α_0 . We set $V_0 = 200$ meV and $r_0 = 7$ nm.

As seen from the figures, the geometrical shape and size of the confinement potential is determined by the structure parameters which have a remarkable effect on the bound-state energies.

5.2 Calculation of Energy Eigenvalues

In order to show the efficiency of FEM, we compare our results for the bound-state energy eigenvalues with those reported in Ref.s Lai (1983) and Miyagi & Someda (2009), denoted $E_{ref(1)}$ and $E_{ref(2)}$ in Table 5.1, respectively. Lai et al. have studied the three-dimensional Gaussian potential with $V_0 = 200$ meV and $r_0 = 1$ nm. The numerical result of ground-state energy for two-dimensional Gaussian potential with $V_0 = 1.404$ meV and $r_0 = 1.404$ nm have been investigated by Miyagi et al. For these systems, the energy eigenvalues found by us are represented as $E_{our(1)}$ and $E_{our(2)}$ in the table, respectively.

The bound-state energy eigenvalues of two-dimensional Gaussian potential obtained by using finite element method considering the effect of ILF are shown below.

Table 5.1 Bound-state energy eigenvalues for Gaussian quantum dot.

n	$-E_{ref(1)}$	$-E_{our(1)}$	$-E_{ref(2)}$	$-E_{our(2)}$
0	341.895	341.8952	0.477	0.4772
1	269.644	269.6445	–	–
2	203.983	203.9835	–	–
3	145.377	145.3779	–	–
4	94.454	94.4577	–	–

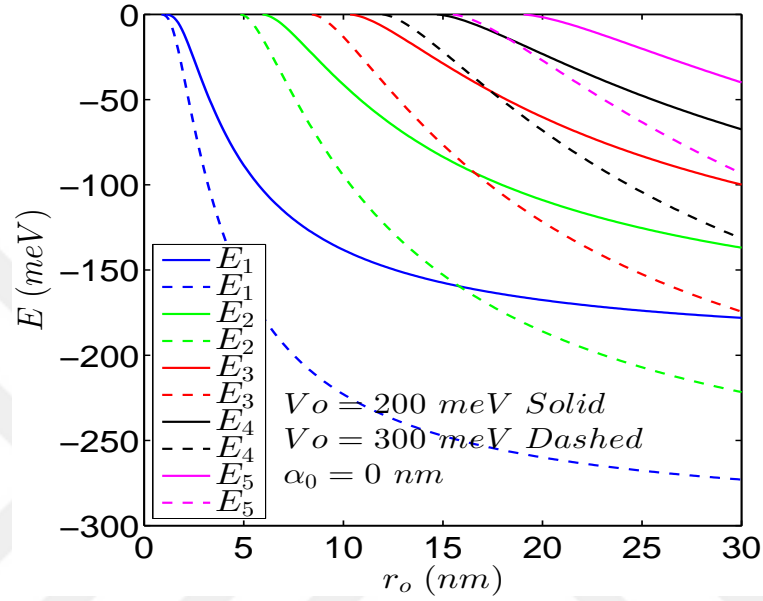


Figure 5.3 Bound-state energies as a function of r_0 for the two values of V_0 in case of $\alpha_0 = 0$ nm.

Figure 5.3 illustrates the energies as a function of r_0 for two different values of V_0 in the absence of an intense laser field. As is deduced from the figure, for smaller values of the range parameter (for deeper potentials) the number of the bound states reduces (increases).

In Figure 5.4, the bound-state energies are plotted with respect to the dot size for different values of α_0 for a constant $V_0 = 250$ meV. We see clearly that, the absolute value of the eigenenergies decrease by increasing the laser-dressing parameter, especially for the lowest states.

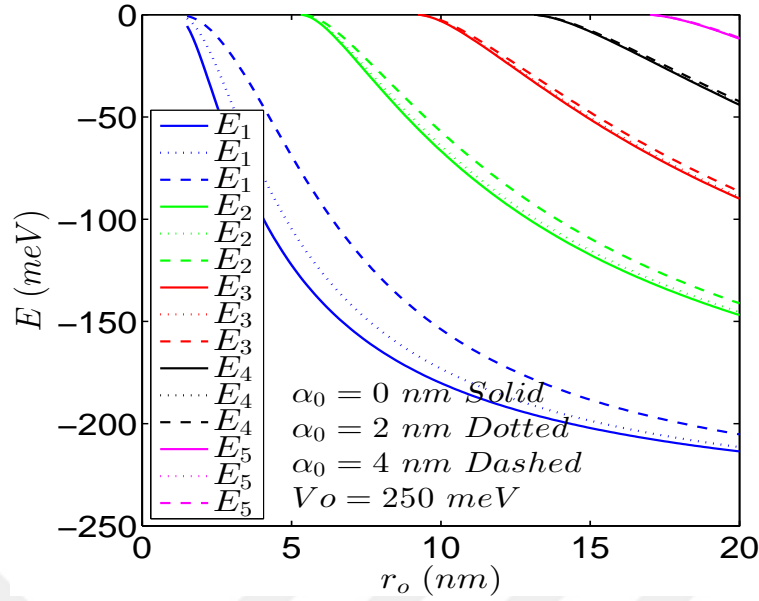


Figure 5.4 Energies as a function of r_0 for the different values of α_0 with $V_0 = 250$ meV.

5.3 The Effects of Intense Laser Field on The Absorption Coefficients

Throughout this work, the optical properties of a two-dimensional quantum dot with Gaussian potential exposed to an intense laser field have been studied. The calculations are realized using the following bulk parameters corresponding to GaAs: $\rho_s = 3.8 \times 10^{22} m^{-3}$ is the electron density, $n_r = \sqrt{\epsilon_r} = 3.6$ is the medium refractive index, $m^* = 0.0665m_0$ is the effective mass (m_0 being the mass of a free electron). What's more, the optical intensity is taken as $I = 0.3 MW/cm^2$.

The magnitudes of the absorption coefficients and refractive index changes are remarkably affected by the dipole matrix element for the transition between the first two-lower lying energy states. In the light of this information, in Figure 5.5 we give the variation of M_{21} . We see that, the matrix element of the electric dipole moment increases slightly with increasing laser-dressing parameter. However, for range parameter of 7 nm this monotonic variation is more pronounced.

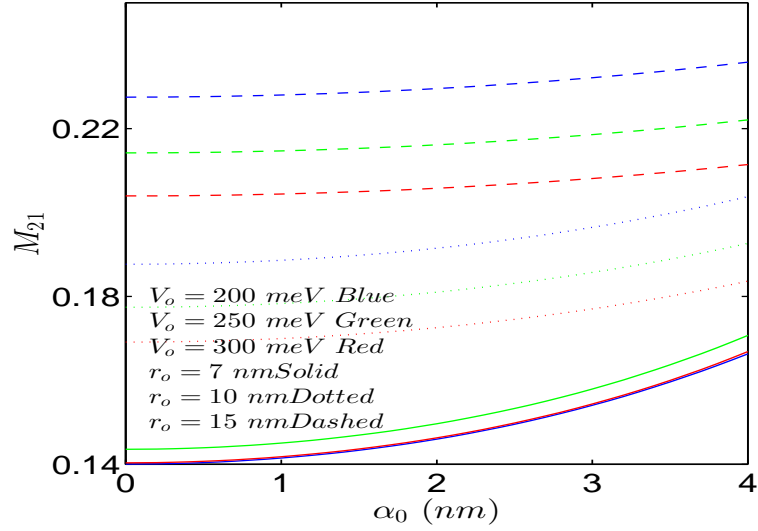


Figure 5.5 The electric dipole moment of the transition between the first state and second state as a function of α_0 for different values of V_0 and r_0 .

Moreover, in Figure 5.6 dependence of the energy difference (transition energy) between the second and first states on α_0 is depicted for different parameters. We can see clearly that while α_0 is increasing the energy difference is decreasing, especially for smaller values of r_0 . On the other hand, for constant α_0 and r_0 the transition energy enhances with increasing V_0 whereas the transition energy reduces with increasing r_0 at constant α_0 and V_0 .

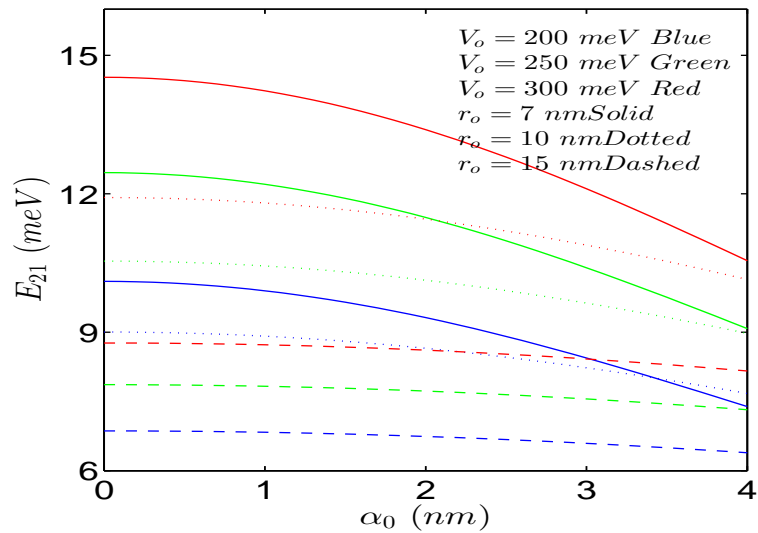


Figure 5.6 The energy difference between the first and second states as a function of α_0 for the different values of V_0 and r_0 .

In order to exhibit the effect of potential geometry on the optical characteristics, initially we investigate the optical absorption coefficients for different values of V_0 and r_0 without taking into account the ILF. Figure 5.7 shows the linear, third-order nonlinear and total absorption coefficient as a function of incident photon energy for different values of V_0 .

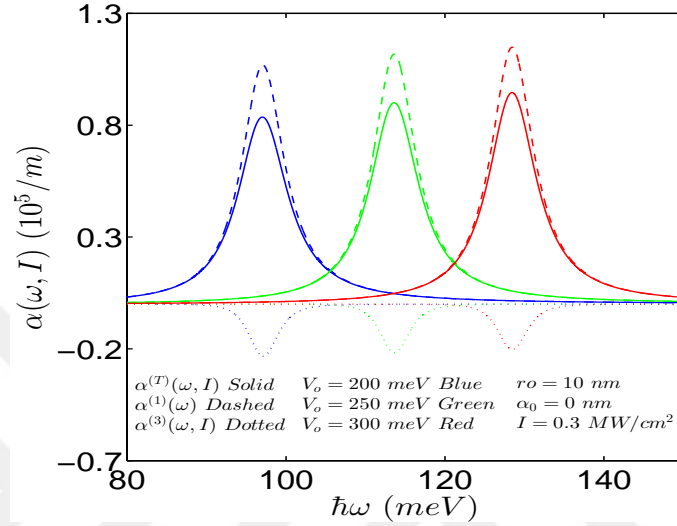


Figure 5.7 Variations of the linear, third-order nonlinear and total AC as a function of the photon energy for the different values of V_0 for $\alpha_0 = 0$ nm, with $r_0 = 10$ nm and $I = 0.3$ MW/cm².

As seen from the figure, while the depth of the dot is increasing, the absorption peak positions shift to higher energies. That's due to the enhancement in the confining potential which leads to the increment in the transition energy with increasing V_0 . Besides, in the case of $r_0 = 7$ nm, further shift in the peak positions toward higher energies values compared with $r_0 = 10$ nm is seen. Furthermore, in this situation, the absorption peak amplitudes increase remarkably with increasing V_0 whereas for $r_0 = 10$ nm slight variation in the peak magnitudes is visible.

In Figure 5.8, in order to see clearly the QD size effect on the optical properties, the linear, third-order nonlinear and total optical AC are shown as a function of the photon energy for different values of r_0 . We can obviously see that as the dot radius increases, the peak positions move to the left side. Providing that $V_0 = 300$ meV, the peaks locations shift to higher energy values.

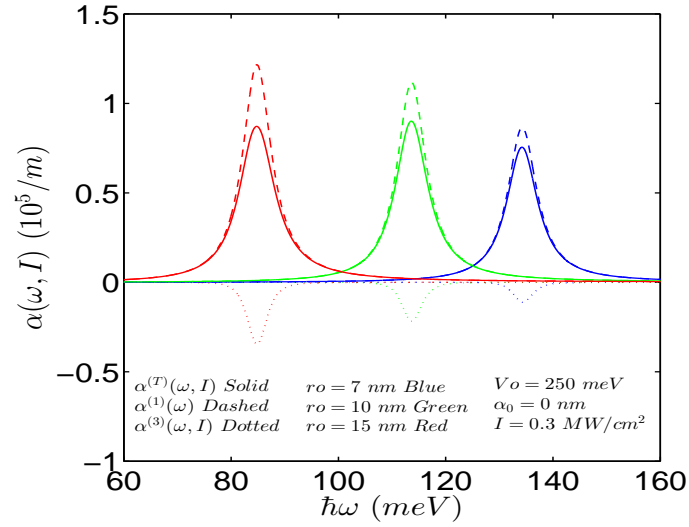


Figure 5.8 Variations of the linear, nonlinear and total AC as a function of the photon energy for the different values of r_0 , for $\alpha_0 = 0$ nm, with $V_0 = 250$ meV and $I = 0.3$ MW/cm².

Modification in the potential profile due to intense laser field causes changes on the optical properties. To reveal the effects of ILF, in Figure 5.9 we illustrate the linear, nonlinear and total AC in a Gaussian QD with $r_0 = 7$ nm and $\alpha_0 = 2$ nm as a function of the photon energy for three different potential depths.

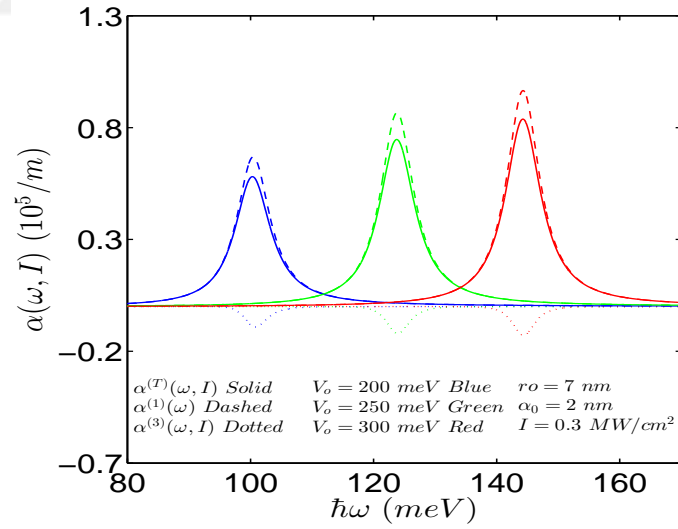


Figure 5.9 Variations of the linear, nonlinear and total AC as a function of the photon energy for the different values of V_0 , with $r_0 = 7$ nm, $\alpha_0 = 2$ nm and $I = 0.3$ MW/cm².

It can be seen that the peak intensity increases just as the potential depth increase. The physical origin is that the transition matrix element increases with increasing the potential depth. If r_0 is taken higher values, the absorption peak positions locate at lower energy region with increased peak magnitude than shown in Figure 5.9.

The effect of varying r_0 by considering ILF defined with $\alpha_0 = 4$ nm, is plotted in Figure 5.10 for the potential depth $V_0 = 300$ meV. We set r_0 to be 7, 10 and 15 nm, respectively.

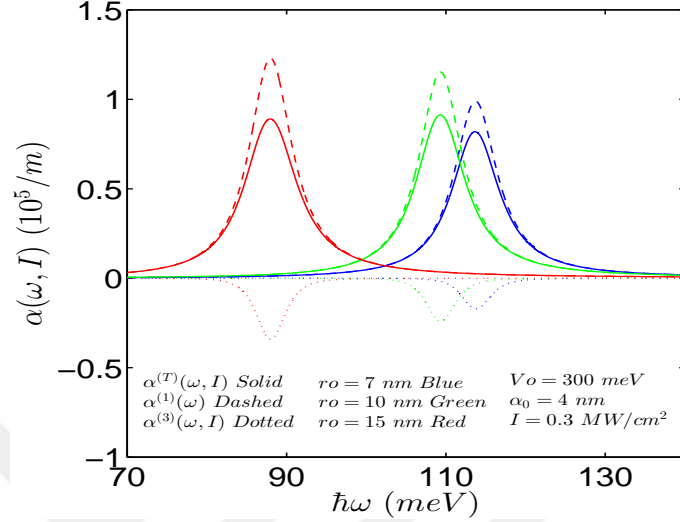


Figure 5.10 Variations of the linear, nonlinear and total AC as a function of the photon energy for the different values of r_0 . We set $V_0 = 300$ meV, $\alpha_0 = 4$ nm and $I = 0.3$ MW/cm².

From this figure, we can see obviously that the peak positions of AC shift to lower photon energies with increasing r_0 . The physical origin is that, with decreasing r_0 the energy difference between the initial and final energy states is increasing. For smaller V_0 values than $V_0 = 300$ meV, the peak positions sit at lower energy region. The reason of this is that the difference between the transition energies decrease with decreasing V_0 . We should note that there is nonmonotonic variation in the peak intensities of all the AC.

In order to elucidate the influence of a circularly polarized, high-frequency ILF on the optical characteristics, in Figure 5.11 we present the linear, third-order nonlinear and total optical AC as a function of the photon energy $\hbar\omega$ for three different laser-dressing parameters. In the figure $V_0 = 200$ meV and $r_0 = 15$ nm are used.

It is readily seen that as the laser-dressing parameter increases, the resonant peak of AC move to the lower energy region. This is because the energy difference between ground and first excited energy states in QD decreases with increasing α_0 . If r_0 is taken 7 nm, the intensity of AC peaks reduces considerably. This is because of that

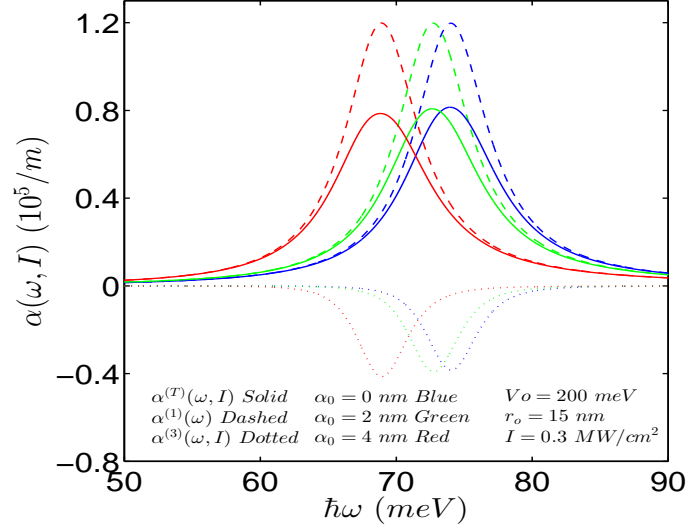


Figure 5.11 Variations of the linear, third-order nonlinear and total AC as a function of the photon energy for the different values of α_0 . We use $V_0 = 200$ meV, $r_0 = 15$ nm and $I = 0.3$ MW/cm².

the transition matrix element decreases with decreasing r_0 . When we take $V_0 = 300$ meV, the AC peak locations shift to higher energies (blue-shift) which is a result of the enhanced energy difference for larger V_0 values.

Demands on materials with low-threshold power for the usage in practical applications imply the large refractive index changes with small incident light intensity (Yu et al., 2011). When the incident optical intensity I is strong enough third-order nonlinear contribution needs to be taken into account. In order to show better the influence of the incident optical intensity I on the total AC, in Figure 5.12 we set $r_0 = 7$ nm, $V_0 = 300$ meV and $\alpha_0 = 4$ nm.

The total AC are plotted as a function of the incident photon energy for six different values of I . The total AC, changes considerably with increasing optical intensity as expected, especially near the resonance frequency. When the incident optical intensity I exceeds a critical value, which demonstrates saturation in the nonlinear term, causes a collapse at center of the total absorption peaks by splitting it into two peaks.

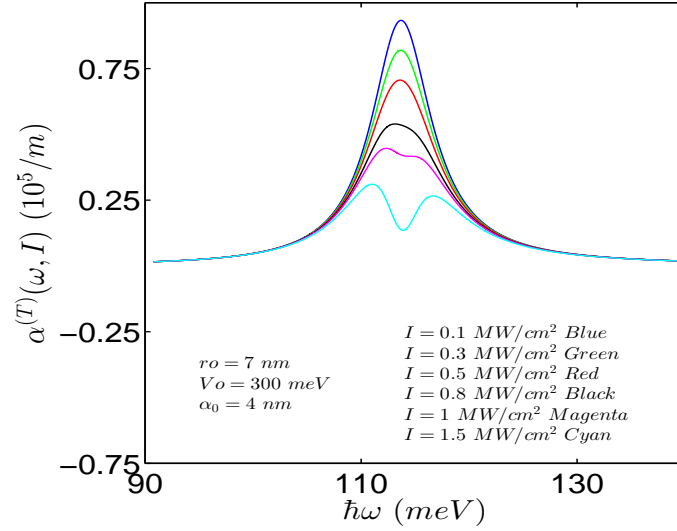


Figure 5.12 Variations of the total AC as a function of the photon energy for the different values of I , with $r_0 = 7$ nm, $V_0 = 300$ meV, $\alpha_0 = 4$ nm.

5.4 The Effects of Intense Laser Field on The Refractive Index Changes

The examination of refractive index changes is important in respect of optoelectronic applications. Accordingly, we will observe the refractive index changes for different parameters in this section.

In Figure 5.13, the linear, third-order nonlinear and total refractive index changes are shown as a function of the incident photon energy for different values of potential depth by using $r_0 = 10$ nm and $\alpha_0 = 0$ nm. As seen in this figure, as the potential depth increases, the magnitudes of the refractive index changes move to higher energies. The main reason for this behavior is that the quantum confinement becomes stronger with increasing potential depth. In addition, for smaller range parameter as $r_0 = 7$ nm the peaks locate at higher energy region with decreasing peak magnitudes.

In order to observe clearly the size-effect on optical properties, in Figure 5.14 we have plotted the linear, third-order nonlinear and total RI changes as a function of photon energy $\hbar\omega$ for three different dot radii $r_0 = 7, 10$ and 15 nm, respectively.

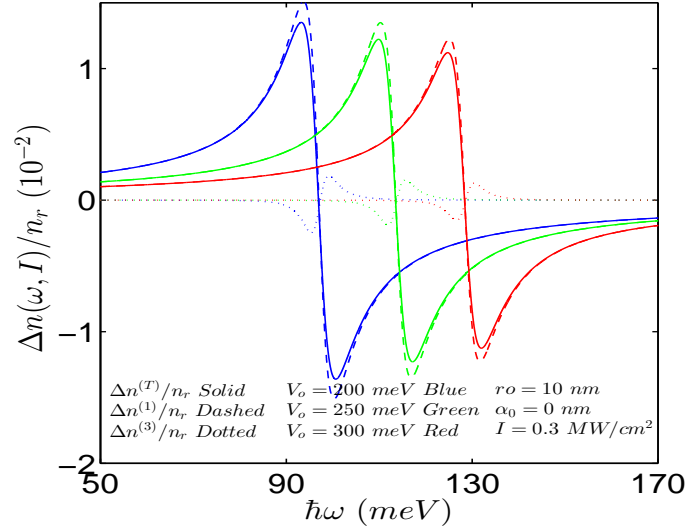


Figure 5.13 The linear, nonlinear and total RI changes as a function of the photon energy for different values of V_0 in the absence of laser field. We set $r_0 = 10$ nm and $I = 0.3$ MW/cm².

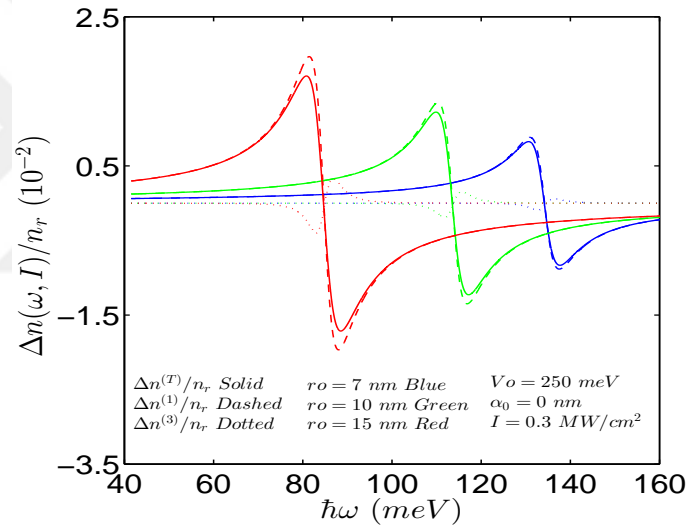


Figure 5.14 The linear, nonlinear and total RI changes as a function of the photon energy for the different values of r_0 in the absence of laser field. Used parameters are $V_0 = 250$ meV and $I = 0.3$ MW/cm².

As we can say from the figure, as the dot radius r_0 increases the peak magnitudes of RI changes increase. The physical origin is that when the dot radius decreases, the QD size will decrease so that the overlapping between the wave functions of the ground and first excited states increases. On the other hand, the wave functions will overflow because of the finite barrier height. Thus, the competition between these two factors will finally decide the peak value of the RI change. If we take $V_0 = 300$ meV, the RI peak positions shift to higher energy region. For, the difference between energy

eigenvalues increases with increasing V_0 .

In order to comprehend the laser-induced changes in the refractive index, in Figure 5.15 the variations of the linear, third-order nonlinear and total RI changes are displayed for the different values of potential depth V_0 with $r_0 = 7$ nm considering the laser-dressing parameter of $\alpha_0 = 2$ nm. The intensity of the incident electromagnetic field is chosen to be $I = 0.3$ MW/cm².

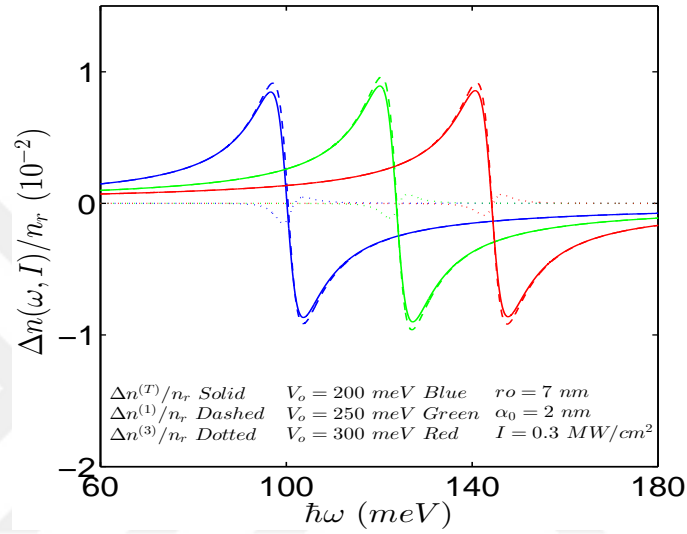


Figure 5.15 Laser field-induced changes on the linear, nonlinear and total refractive index as a function of the photon energy for the different values of V_0 with $r_0 = 7$ nm where the laser-dressing parameter is chosen as $\alpha_0 = 2$ nm.

It is seen that, the increment in the potential depth shifts the peak positions to higher frequencies. When the system is irradiated with ILF, the depth of the potential becomes shallows which results in observation of red-shifted resonant peaks. For stronger confinements (increasing V_0), the difference between the energy levels increases which eventually causes the anomalous regions at higher energies. If r_0 is taken higher values, the RI peak positions locate at lower energy region which is directly related to decrement in the energy difference.

Figure 5.16 illustrates the linear, third-order nonlinear and total RI changes as a function of the photon energy for varying values of the dot radius for $V_0 = 300$ meV , $\alpha_0 = 4$ nm and $I = 0.3$ MW/cm².

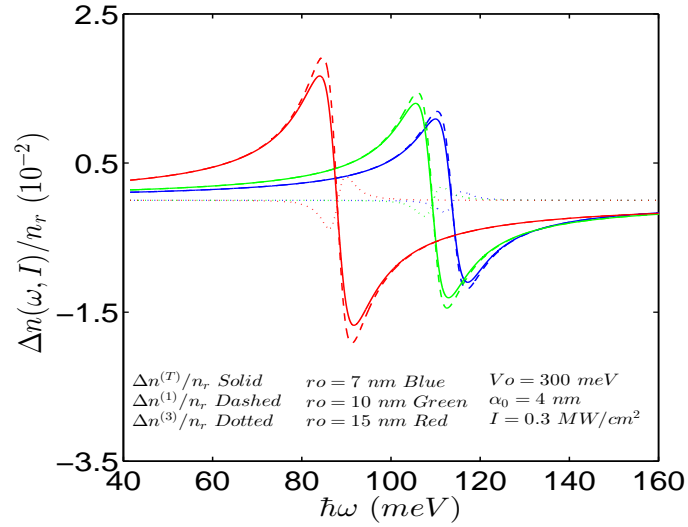


Figure 5.16 Dependence of the linear, nonlinear and total RI changes on the range parameter r_0 . Potential depth with $V_0 = 300$ meV is chosen and laser-dressing parameter is set to be $\alpha_0 = 4$ nm.

We can see from the figure that the peaks of RI changes shift toward lower energies with increasing r_0 . This red-shift is because of the fact that the energy difference between the ground state and the first excited state in the QD decreases with increasing dot radius. As long as V_0 is taken lower values, due to the decrement in the difference between energy eigenvalues, the peak location moves to lower energy values.

So as to show better the influence of the laser effect on the refractive index changes, in Figure 5.17, the linear, third-order nonlinear and total refractive index changes are plotted as a function of incident photon energy for three different laser-dressing parameters. In this figure, the barrier height and the dot radii are set to be $V_0 = 200$ meV and $r_0 = 15$ nm, respectively.

It is obvious that, as the strength of laser field increases, refractive index changes shift towards lower energies. This happens because of the decrease in the energy differences between the first and second bound-state energy levels with increasing α_0 . For lower r_0 or higher V_0 , the RI peak positions move to higher energy region. This reason is that the difference between the energy levels increase with reducing r_0 or ascending V_0 .

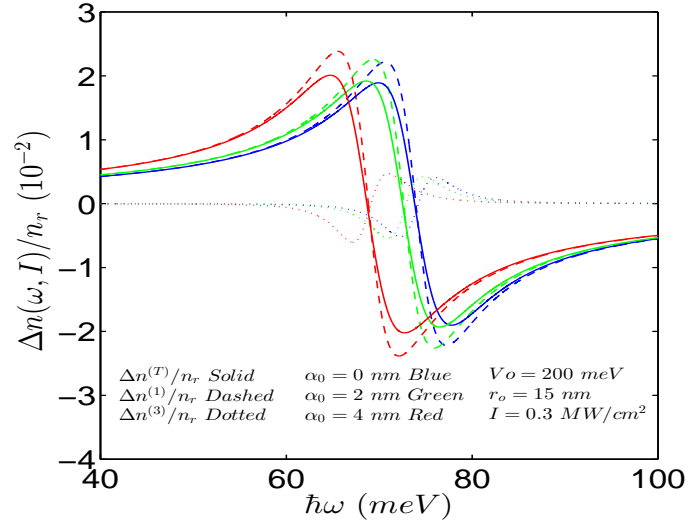


Figure 5.17 The effect of laser-dressing parameter on the linear, third-order nonlinear and total RI changes as a function of the photon energy. Quantum dot with $V_0 = 200$ meV and $r_0 = 15$ nm is chosen.

Finally, in Figure 5.18, in order to see clearly the influence of the incident optical intensity I on the total optical refractive index change, we set $r_0 = 7$ nm, $V_0 = 300$ meV and $\alpha_0 = 4$ nm for six different values of I .

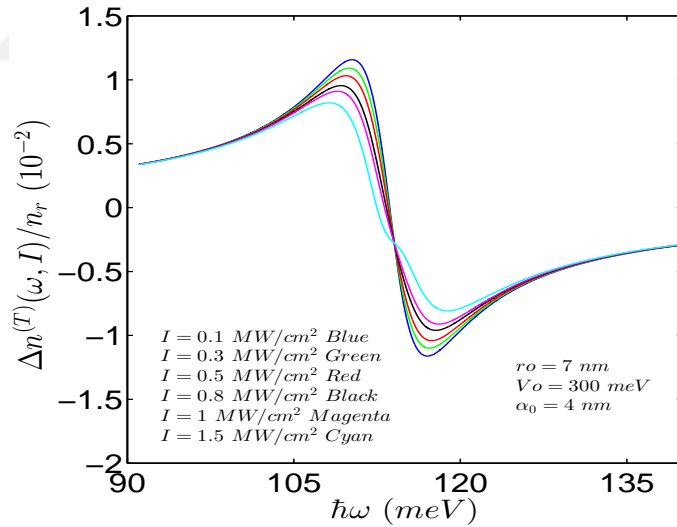


Figure 5.18 The total RI changes as a function of the photon energy for the different values of I , with $r_0 = 7$ nm, $V_0 = 300$ meV, $\alpha_0 = 4$ nm.

In this figure, we see that as the intensity of the optical field increases, the peak heights of the total RI changes shorten and anomalous region spreads out. This situation can be attributed to the enhancing third-order nonlinear effects.

CHAPTER SIX

CONCLUSION

The propose of this thesis is to investigate theoretically the effects of intense laser field on the nonlinear optical properties of two-dimensional quantum dot system. The system described by the Gaussian confinement potential is exposed to a high-frequency intense laser field with circular polarization. Within the framework of non-perturbative approach and by means of Kramers-Henneberger unitary translational transformation and Fourier-Floquet serial expansion, the motion of an electron is described with time-independent Schrödinger equation including laser-dressed potential.

Electronic properties of the system have been found by the numerical solution of the Schrödinger equation by using finite element method based on Galerkin's approach. Nonlinear optical properties of the system have been extracted from the compact-density matrix approach and iterative procedure. Energy eigenvalues and corresponding eigenfunctions as well as the linear and third-order nonlinear optical absorption coefficients and refractive index changes are investigated for various values of the structure parameters and laser field strengths.

Numerical results show that, in the presence of intense laser field the confinement potential is strongly affected by the structure parameters V_0 (depth of the potential) and r_0 (range parameter). With increasing values of laser-dressing parameter, the width of the confinement potential expands and furthermore, the depth of potential decreases. These modifications in confinement potential cause the changes in the energy levels and corresponding eigenfunctions. We demonstrated that optical absorption coefficients and refractive index changes are blue-shifted (red-shifted) for increasing value of V_0 (r_0). Further shift in the resonant peak toward the lower energy region is observed when the laser field in turned on. These variations are more pronounced for smaller range parameters. Moreover, increment in the incident optical intensity results in the strengthening of the nonlinear contributions which leads to a bleaching in the resonant peaks.

Consequently, our results demonstrate that the nonlinear optical properties of two-dimensional Gaussian quantum dot are influenced by the strength of the intense laser field and structure parameters. These findings may make a contribution for utilization of the quantum-size effect in optoelectronic devices and can assist in designing of systems with controllable optical transitions.



REFERENCES

- Ahn, D., & Chuang, S.-L. (1987). Calculation of linear and nonlinear intersubband optical absorptions in a quantum well model with an applied electric field. *IEEE Journal of Quantum Electronics*, *QE-23*(12), 2196–2204.
- Bauer, D. (2006). *Theory of intense laser-matter interaction*. Max-Planck-Institut für Kernphysik.
- Boyd, R. W. (2008). *Nonlinear optics*. (3rd ed.). Academic Press.
- Brandi, H. S., Latgé, A., & Oliveira, L. E. (2004). Laser effects on donor states in low-dimensional semiconductor heterostructures. *Physical Review B*, *70*, 153303.
- Buchanan, G. R. (1995). *Schaum's outline of theory and problems of finite element analysis*. (1st ed.). McGraw-Hill.
- Colton, D., & Kress, R. (1998). Inverse acoustic and electromagnetic scattering theory. *Applied Mathematical Sciences*, *93*.
- Duque, C. A., Mora-Ramos, M. E., Kasapoglu, E., Ungan, F., Yesilgul, U., Sakiroglu, S., Sari, H., & Sökmen, I. (2013). Impurity-related linear and nonlinear optical response in quantum-well wires with triangular cross section. *Journal of Luminescence*, *143*, 304–313.
- Ehsanfard, N., & Vahdani, M. R. K. (2015). Intersubband optical absorption coefficients and refractive index changes in a gaussian spherical quantum dot. *International Journal of Theoretical Physics*, *54*, 2419–2435.
- Garmire, E., & Kost, A. (1999). *Nonlinear optics in semiconductors II*, vol. 59. (1st ed.). Academic Press.
- Gavrila, M. (2002). Atomic stabilization in superintense laser field. *Journal of Physics B*, *35*, R147–R193.
- Gomez, S. S., & Romero, R. H. (2009). Few-electron semiconductor quantum dots with gaussian confinement. *Central European Journal of Physics*, *7*(1), 12–21.

- Gül, D. (2014). *Nonlinear optical properties of a two-dimensional quantum pseudo-dot system under intense laser field*. Master's Thesis, Dokuz Eylül University.
- Hanna, J. R., & Rowland, J. H. (2008). *Fourier series, transforms, and boundary value problems*. (2nd ed.). Dover Publications.
- Jonsson, F. (2003). *Lecture notes on nonlinear optics*. Lectures presented at the Royal Institute of Technology, Department of Laser Physics and Quantum Optics.
- Kavruk, A. E., Sahin, M., & Koc, F. (2013). Linear and nonlinear optical properties of $GaAs/Al_xGa_{1-x}As/GaAs/Al_yGa_{1-y}As$ multi-shell spherical quantum dot. *Journal of Applied Physics*, *114*(183704).
- Khordad, R. (2012). Pressure effect on optical properties of modified gaussian quantum dot. *Physica B*, *407*, 1128–1133.
- Lai, C. (1983). On the schrödinger equation for the gaussian potential $-Aexp(-hr^2)$. *Journal of Physics A: Mathematical and General*, *16*, L181–L185.
- Lima, F. M. S., Amato, M. A., Nunes, O. A. C., Fonseca, A. L. A., Enders, B. G., & da Silva, E. F. (2009). Unexpected transition from single to double quantum well potential induced by intense laser fields in a semiconductor quantum well. *Journal of Applied Physics*, *105*, 123111.
- Lima, F. M. S., Nunes, O. A. C., Amato, M. A., Fonseca, A. L. A., & da Silva, E. F. (2008). Dichotomy of the exciton wave function in semiconductors under intense laser fields. *Journal of Applied Physics*, *103*, 113112.
- Liu, G., Guo, K., & Wang, C. (2012). Linear and nonlinear intersubband optical absorption in a disk-shaped quantum dot with a parabolic potential plus an inverse squared potential in a static magnetic field. *Physica B*, *407*, 2334–2339.
- Logan, D. L. (2007). *A first course in the finite element method*. (4th ed.). Thomson.
- Lu, L., Xie, W., & Hassanabadi, H. (2011a). The effects of intense laser on nonlinear propoerties of shallow donor impurities in quantum dots with the woods-saxon potential. *Journal of Luminescence*, *131*, 2538–2543.

- Lu, L., Xie, W., & Hassanabadi, H. (2011b). Laser field effect on the nonlinear optical properties of donor impurities in quantum dots with gaussian potential. *Physica B*, 406, 4129–4134.
- Mills, D. (1998). *Nonlinear optics*. (2nd ed.). Springer-Verlag Berlin Heidelberg.
- Miyagi, H., & Someda, K. (2009). Unified view of low- and high-frequency regimes of atomic ionization in intense laser fields. *Physical Review A*, 80(023416).
- Niculescu, E., & Burileanu, L. (2010). Nonlinear optical absorption in inverse v-shaped quantum wells modulated by high-frequency laser field. *The European Physical Journal B*, 74, 117–122.
- Nikishkov, G. (2010). *Programming finite elements in java*. (1st ed.). Springer-Verlag London.
- Onate, E. (2009). *Structural analysis with the finite element method linear statics*, vol. 1. (1st ed.). Springer Netherlands.
- Ozturk, E., & Sokmen, I. (2014). Nonlinear intersubband transitions in a parabolic and an inverse parabolic quantum well under applied magnetic field. *Journal of Luminescence*, 145, 387–392.
- Pont, M., & Gavrilă, M. (1990). Stabilization of atomic hydrogen in superintense, high-frequency laser fields of circular polarization. *Physical Review Letters*, 65(19), 2362–2365.
- Protopapas, M., Keitel, C. H., & Knight, P. L. (1997). Atomic physics with super-high intensity lasers. *Reports on Progress in Physics*, 60, 389–486.
- Razeghi, M. (2009). *Fundamentals of solid state engineering*. (3rd ed.). Springer US.
- Safarpour, G., Zamani, A., Izadi, M., & Ganjipour, H. (2014). Laser radiation effect on the optical properties of a spherical quantum dot confined in a cylindrical nanowire. *Journal of Luminescence*, 147, 295–303.
- Sakirođlu, S., Urgan, F., Yesilgul, U., Mora-Ramos, M., Duque, C., Kasapoglu, E., Sari, H., & Sökmen, İ. (2012). Nonlinear optical rectification and the second and

- third harmonic generation in pöschl-teller quantum well under the intense laser field. *Physics Letters A*, 376, 1875–1880.
- Saravanamoorthy, S., Peter, A. J., & Lee, C. W. (2014). Optical absorption coefficients in a $CdSe/Pb_{1-x}Cd_xSe/CdSe$ spherical quantum dot quantum well nanostructure. *Physica E*, 63, 337–342.
- Sarikurt, S. (2013). *Electronic structure of parabolic confining quantum wires with rashba and dresselhaus spin-orbit coupling in a perpendicular magnetic field*. Ph.D. Thesis, Dokuz Eylül University.
- Sutherland, R. L. (2003). *Handbook of nonlinear optics*. (2nd ed.). Marcel Dekker, Inc.
- Tiutiunnyk, A., Tulupenko, V., Mora-Ramos, M., Kasapoglu, E., Urgan, F., Sari, H., Sökmen, I., & Duque, C. A. (2014). Electron-related optical responses in triangular quantum dots. *Physica E*, 60, 127–132.
- Urgan, F., Yesilgul, U., Şakiroğlu, S., Kasapoglu, E., Sari, H., & Sökmen, I. (2010). Effects of an intense, high-frequency laser field on the intersubband transitions and impurity binding energy in semiconductor quantum wells. *Physics Letters A*, 374, 2980–2984.
- Wen-Fang, X. (2007). Three-electron quantum dots in zero magnetic field. *Communication in Theoretical Physics*, 48, 1115–1118.
- Xie, W. (2008a). Linear and nonlinear optical properties of a hydrogenic donor in spherical quantum dots. *Physica B*, 403, 4319–4322.
- Xie, W. (2008b). Nonlinear optical properties of a hydrogenic donor quantum dot. *Physics Letter A*, 372, 5498–5500.
- Xie, W. (2010a). Linear and nonlinear optical absorptions of an exciton in a quantum ring. *Physica E*, 43, 49–53.
- Xie, W. (2010b). Optical properties of an off-center hydrogenic impurity in a spherical quantum dot with gaussian potential. *Superlattices and Microstructures*, 48, 239–247.

Xie, W. (2011). Optical absorption and refractive index of an exciton quantum dot under intense laser radiation. *Physica E*, 43, 1704–1707.

Young W. Kwon, H. B. (1997). *The finite element method using matlab*. (1st ed.). CRC Press.

Yu, F.-M., Chen, H.-B., & Zhou, L.-P. (2011). Polaron effects on the change of refractive index in asymmetrical quantum wells. *Chinese Journal of Physics*, 49(2), 629–638.

Zhang, L., Yu, Z., Yao, W., Liu, Y., & Feng, H. (2011). Optical properties of *GaN/AlN* quantum dots under intense laser field. *SPIE-OSA-IEEE*, 8308, 830813.